ASDJournal (2018), Vol. 6, No. 1, pp. 43–72

Unsteady Aerodynamic Model Order Reduction for Aeroservoelastic Optimisation by Balanced Proper Orthogonal Decomposition and the use of Synthetic Mode Shapes

(Received: November 11, 2018. Revised: April 12, 2019. Accepted: May 1, 2019)

Simon Binder[1,2]
Andreas Wildschek[3]
Roeland De Breuker[2]

Abstract
The combined optimisation of aircraft structures and active control systems in early design stages requires low-order unsteady aerodynamic models that are robust to structural and control surface layout modifications. A combination of the balanced proper orthogonal decomposition with the concept of synthetic modes is proposed and different formulations for the generation of synthetic modes are given. The models resulting from the proposed procedure are tested for their suitability and accuracy in aero(servo)elastic analyses (stability assessment, continuous turbulence loads and calculation of control surface transfer functions) of a tube-wing aircraft configuration. The results indicate that the number and type of synthetic modes have a significant influence on the achievable accuracy and the accuracy per order of the resulting reduced order model. At a required accuracy of 10^{-3}, the most suitable set of synthetic modes is based on radial basis functions and reduces the aerodynamic model order by about two orders of magnitude while still being able to handle structural and control surface layout modifications.

1. Introduction

The ever-increasing demand on cost and fuel efficiency are driving the development of aircraft with high aspect ratio wings, lightweight structures and technologies such as active control. The resulting increased influence of structural flexibility along with the increased interaction between structural dynamics and aerodynamics require new ways of working in early stages of aircraft design. Also, the growing use of active control methods such as gust load control or aeroelastic stability control must be considered as early as possible to achieve more optimal designs. One possibility to master this challenge is the use of computational methods and multidisciplinary design optimisation (MDO). The integration of a multitude of disciplines enables the uncovering of potentials that cannot be achieved through classical iterative design methods. A part of the integrated design of future aircraft is known as the field of aeroservoelasticity incorporating aero-, structural and control system dynamics. Integrated models for analysis and optimisation that originate in this field are often very complex and computationally costly to simulate. For the optimisation problems to be carried out in the conceptual and preliminary design stages, fast turnaround times are required to enable the assessment of many configurations, parameter variations and trade-offs. Typically, the modelling of transient aerodynamics involves the highest complexity (i.e. states in the resulting model) among the various disciplines of aeroservoelasticity and thus offers the highest potential regarding the reduction of turnaround times and computational effort. The present work is thus concerned with finding a solution to significantly reduce

[1] Department of Aeromechanics Systems, Airbus Defence and Space GmbH, 81663, Munich, Germany
[2] Faculty of Aerospace Engineering, Department of Aerospace Structures and Materials, Delft University of Technology, 2629 HS, Delft, The Netherlands
[3] Aircraft Control Domain, Airbus Operations SAS, 31060, Toulouse, France

doi:10.3293/asdj.2018.49

the dimensionality of the aerodynamic model while ensuring the required accuracy in aeroelastic analyses even in the presence of considerable parameter variations of the concept to be optimised. This solution shall enable the efficient integrated optimization of active control systems (e.g. for load alleviation or flutter suppression) along with the primary wing structure (i.e. layout and dimensions of wing skins, spars, stiffeners and ribs). Special focus is therefore placed on assuring the accuracy of aeroelastic analyses in the presence of parameter variations of the structure and the control systems. These variations include on the one hand the variation of the position and size of control surfaces and on the other hand the variation of the stiffness and mass distribution of the primary structure. In aircraft design, analyses of the aeroservoelastic model (stability, flight loads and control law synthesis) must be carried out at many flight points to verify a design point across the targeted flight envelope. The number of equations required for the generation of the models ranges from $10^3 - 10^4$ (potential flow based methods) to $> 10^6$ (higher order methods) solely for the aerodynamics. Order reduction before analysis is inevitable to enable the many studies in a reasonable time frame. On the global or system level, many conventional approaches exist which originated from control engineering. The most intuitive method is simply truncating certain states that are not significantly influencing the dynamics. The selection, however, requires precise knowledge of the individual states and how they contribute to the overall dynamics. A selection might be based on Another method for the reduction of a dynamic model is the modal truncation. Here the selection is based on an eigenanalysis of the model and a transformation on a selected subset of eigenmodes yields the reduced order model. While the eigendynamics of the full order model might be contained in the reduced order model, the input-state and state-output behaviour of the dynamic system are not considered during the selection of the subset of eigenmodes. An important and widely used method that considers the input-state and the state-output behaviour is the Balanced Truncation (BT). Here, the system is first transformed in a balanced form so that the resulting states are equally controllable as observable [1]. Then the model order is reduced by keeping only the most controllable and observable states. The method has proven to be very efficient while producing models which closely match the input-output behaviour of the full order models. However, for large systems as in aeroservoelasticity, this kind of methods are often not directly applicable due to limited computational resources. Besides, after transforming the integrated model, the individual equations can no longer be associated with the different disciplines. Thus, usually, an order reduction on the discipline level is performed before the global reduction with methods suitable for the different properties of the models (e.g. Guyan and modal reduction for structural models) [2].

In the field of fluid dynamics, several methods were developed in the past decades. Three of the most prominent examples are the Proper Orthogonal Decomposition (POD), also known as KarhunenLoève decomposition, the Balanced Proper Orthogonal Decomposition (BPOD) and the Eigensystem Realization Algorithm (ERA).

The mentioned methods fall into the category of snapshot-based methods in which a limited collection of data from simulations or experiments is used. In the POD, the snapshots are used to compute a vector basis which optimally approximates the collected state snapshot data [3]. A combination of the POD and the balanced truncation has been presented by Rowley forming the BPOD [4]. To overcome the limitation that the POD based models can only reflect the input-state behaviour and not the state-output behaviour, both, snapshot simulations of primal and the adjoint or dual system are used to compute a transformation that approximately balances the system. The ERA algorithm tries to find a state-space realisation of a system reflecting the collected input-output snapshot data in a balanced form. Ma et al. compare the BPOD and the ERA algorithm yielding that theoretically, both methods produce identical

ROMs [5]. However, an advantage of the BPOD is that it produces a set of bi-orthogonal vectors with which the full order model can be reconstructed from the reduced order model, while the ERA algorithm produces only the ROM without information about the relation of the resulting states to the original states. In other words, in case the full order system is given including its adjoint form, less information gets lost during the model order reduction by BPOD. The BPOD was successfully applied in reducing aerodynamic models of airfoils, cascades and wings [6], [7].

For the generation of aerodynamic reduced order models used in aeroelastic applications, all the previously described methods require the structural and flight dynamic degrees of freedom to be reduced to a finite set of generalised coordinates to reduce the number of in- and outputs of the aerodynamic model. Thus, the resulting model is only valid and accurate for these structural degrees of freedom. In sizing-type aeroelastic optimisation (i.e. for a fixed topology and shape), the mass and stiffness distribution and thus the structural mode shapes change during the design. It is therefore desirable to create one ROM which is robust enough to capture all expected variations in the structural and flight dynamic degrees of freedom. Fenwick et al. presented a study in which the resulting reduced order model was interpolated from a previously created data basis across the structural parameter range [8]. In optimisations with a large number of structural parameters such as aircraft structure optimisations, this requires a large amount of models to be created before the optimisation. A suggestion to account for arbitrary structural modifications is to use significantly more mode shapes of the basis model for the generation of the reduced order model than used in the aeroelastic analysis [9]. This approach requires the basis mode shapes to represent all structural modifications occurring during the optimisation. Another method is to augment the basis mode shapes by the introduction of fictitious masses [10]. The modal basis of the overall structure is enriched by the integration of modes of the substructure where structural modifications are expected or planned. The method has been especially useful in augmenting dynamic models of fighter aircraft to enable the efficient flutter analysis of numerous loading conditions [11]. Furthermore, the method was successfully applied to include local deformations of actuators and their attachment structure in low dimensional modal representations of the overall structure [12]. However, it is required that all possible structural modifications and their locations are known beforehand to ensure the required robustness.

Instead of utilising the mode shapes of the basis model, artificial mode shapes (also referred to as prescribed or synthetic mode shapes) may be used which are not related to the basis structural model. Voss et al. compared the use of different functions and polynomials for generation of synthetic mode shapes finding that only ten synthetic mode shapes are required to approximate the first 50 structural eigenmodes of a transport aircraft regarding the Modal Assurance Criterion (MAC) [13]. However, the different types used have not been compared concerning their suitability to approximate the aeroelastic behaviour. With respect to snapshot based model order reduction techniques, Zhang et al. reproduced the snapshot data for the current mode shapes by reprojecting them on the snapshot data generated with Radial Basis Function (RBF) based synthetic mode shapes [14]. Winter et al. created mode shapes based on Chebyshev polynomials and RBFs to establish a ROM which is robust to structural variations [15]. Their studies include a qualitative comparison of the two different methods for basis mode shape generation concerning the accuracy of generalised aerodynamic forces generated with the resulting ROM.

The mentioned examples study the accuracy of the resulting ROMs concerning their frequency response or flutter point of an isolated wing. All the examples deal with purely structural modifications of the basis model. In aeroservoelastic optimisations carried out in early design stages of aircraft, also the position and size of control surfaces may be varied. The robustness of ROMs to changes of the control surface layout has not been studied so far.

In this work, first, the basic concept of BT, POD and BPOD are reviewed. The BPOD is then combined with the concept of synthetic mode shapes. Therefore, three different methods for synthetic mode shape generation based on RBF, Chebyshev polynomials and zonal subdivision are formulated for full aircraft configurations including wings, horizontal and vertical tail. These synthetic modal bases are used in the process of the aerodynamic model order reduction. After the reduction process, the aerodynamic ROMs are combined with the flight dynamic and structural equations of motion forming the integrated aeroelastic model. Subsequently, flutter point, continuous turbulence loads and control surface transfer functions are computed in the presence of structural (mass and stiffness distribution) and control surface layout variations (size and location of the control surfaces). The influence of the number of synthetic mode shapes used for the generation of training data on the accuracy of the resulting ROMs is studied. Finally, a quantitative comparison of the accuracy is made between the different approaches for synthetic mode shape generation used for the training data generation.

2. Methodology

Each component or discipline involved in the field of aeroservoelasticity (aero-, flight- and structural dynamics as well as sensors and actuators) can be modelled as a dynamic system. The term modelling refers to the derivation of mathematical equations describing the behaviour of those systems. The result is mostly a set of coupled ordinary differential equations (ODE) or partial differential equations (PDE). In the latter case, the conversion to systems of ODEs is often done with discretisation methods as finite elements, volumes, differences or boundary element methods. As the solution of non-linear ODEs is complex and linear approximations can be obtained around a specific equilibrium point. For each component in aeroservoelasticity, eventually, the result is a set of homogeneous, linear ODEs (also known as Linear Time-Invariant (LTI) system) which can be cast into a state space representation of the form:

$$\begin{aligned}\dot{\mathbf{x}} &= \mathbf{A}\mathbf{x} + \mathbf{B}\mathbf{u} \\ \mathbf{y} &= \mathbf{C}\mathbf{x} + \mathbf{D}\mathbf{u}\end{aligned} \tag{1}$$

with the state vector $\mathbf{x} \in \mathbb{R}^n$, the output vector $\mathbf{y} \in \mathbb{R}^q$ and the input vector $\mathbf{u} \in \mathbb{R}^p$ where n, p and m are the number of states, outputs and inputs of the state space system. The physical interpretation of inputs to an aerodynamic model used in aeroelastic applications are variations of boundary conditions due to surface motion or external disturbances. The outputs correspond to the variation in pressure distributions across the surfaces. The exact interpretation of the states depends on the underlying numerical modelling technique. For potential flow methods as they are most commonly used in subsonic aero(servo)elastic applications, the states can be associated to the unsteady interaction between the wake and the lifting surfaces (also known as lag states). Models representing the unsteady aerodynamics of full aircraft configurations can be large and costly to simulate. Techniques reducing the number of states are referred to as model order reduction methods. All methods target the realisation of models that reproduce the behaviour of interest as precisely as possible with a lower number of states and equations. The fundamental model order reduction methods have their origin in the field of control engineering in the late last century [16]. The methods forming the basis of this paper are the BT and the POD. Both methods are projection based methods that reduce the space in which the differential equations are solved by projection on a new set of basis vectors:

$$\mathbf{x}_r = \mathbf{\Phi}_r \mathbf{x} \tag{2}$$

with the reduced state vector $\mathbf{x}_r \in \mathbb{R}^{k<n}$ and the reduction basis $\mathbf{\Phi}_r \in \mathbb{R}^{k\times n}$. The resulting ROM is then given by:

$$\begin{aligned}\dot{\mathbf{x}}_r &= \tilde{\mathbf{A}}\mathbf{x}_r + \tilde{\mathbf{B}}\mathbf{u} = \mathbf{\Phi}_r^{-1}\mathbf{A}\mathbf{\Phi}_r\mathbf{x}_r + \mathbf{\Phi}_r^{-1}\mathbf{B}\mathbf{u} \\ \mathbf{y} &= \tilde{\mathbf{C}}\mathbf{x}_r + \mathbf{D}\mathbf{u} = \mathbf{C}\mathbf{\Phi}_r\mathbf{x}_r + \mathbf{D}\mathbf{u}\end{aligned} \tag{3}$$

In order to outline the basis for the present work, the following section (2.1) presents a quick review of the concepts of BT and POD followed by the introduction of the combined BPOD. In Section 2.2 the use of synthetic mode shapes for the reduction of large aerodynamic systems used in aeroservoelastic applications is proposed and three different types of synthetic mode shapes are formulated for full aircraft configurations. A summary of the resulting combined procedure is presented in Section 2.3.

2.1 Model Reduction by Balanced Proper Orthogonal Decomposition

Balanced Truncation The concept of balancing was initially developed by Moore in the balanced truncation with the idea to reduce the state space onto a subspace spanned by the most controllable and observable states [1]. Therefore, Gramians are computed which can be used to quantify the contribution of the individual states to the input-state and state-output behaviour. The controllability Gramian $\mathbf{W}_c$ used for the quantification of the input-state contribution of a stable system is given by:

$$\mathbf{W}_c = \int_0^\infty e^{\mathbf{A}t}\mathbf{B}\mathbf{B}^T e^{\mathbf{A}^T t}dt \tag{4}$$

An interpretation of Eq. 4 is that the controllability Gramian equals the infinite integral of the outer product of impulse state responses for every input to the system. The actual quantification is done by computing the Singular Value Decomposition (SVD) of the Gramian:

$$\mathbf{W}_c = \mathbf{U}_c\mathbf{\Sigma}_c\mathbf{V}_c^T \tag{5}$$

where $\mathbf{\Sigma}_c$ contains the singular values σ_c on its diagonal ($\mathbf{\Sigma}_c = \text{diag}(\sigma_{c,1}...\sigma_{c,n})$ with $\sigma_{c,1} \geq \sigma_{c,2} \geq ... \geq \sigma_{c,n}$) and $\mathbf{U}_c$ as well as $\mathbf{V}_c$ the corresponding left and right-singular vectors as columns. The singular value σ_i then quantifies the controllability of the state described by the i-th column of $\mathbf{U}_c$.

The observability Gramian $\mathbf{W}_o$ for determination of the relative state-output importance is given similarly:

$$\mathbf{W}_o = \int_0^\infty e^{\mathbf{A}^T t}\mathbf{C}^T\mathbf{C}e^{\mathbf{A}t}dt \tag{6}$$

According to the principle of duality, the observability Gramian equals the controllability Gramian of the adjoint ($\bar{\cdot}$) or dual system whose state equation is given by:

$$\dot{\bar{\mathbf{x}}} = \mathbf{A}^T\bar{\mathbf{x}} + \mathbf{C}^T\bar{\mathbf{u}} \tag{7}$$

with $\bar{\mathbf{x}}$ being the dual system state vector.

A system is in its balanced form when the resulting reduced states are equally observable as controllable, i.e. the singular values of the Gramians coincide. The transformation that balances the system is found by an eigenanalysis of the product $\mathbf{W}_c\mathbf{W}_o$. When the system is in its balanced form, a reduced order model is obtained by truncation of the least controllable and observable states. For further information, the reader is referenced to [1], or to [17] for the numerically more reliable Square Root Balanced Truncation.

Usually, the Gramians are computed by solving the Lyapunov equation. However, the algorithm used for the solution is computationally expensive, and the effort grows cubically with the number of states [18]. Thus, for large systems, the standard balanced truncation is practically not feasible. In the past decades, many methods have been developed with the aim to realise approximately balanced ROMs for such large-scale systems. Many of those methods make use of simulation snapshots as they can be obtained for all kinds of underlying dynamical systems. One of those methods is the use of empirical Gramians based on simulation data for the computation of the balancing transformation. Assuming the empirical Gramians represent a good approximation of the exact Gramians, the resulting truncated balanced realisation models are very close to the models obtained by using exact Gramians. Moore already used time sampled simulation data for the computation of the Gramians instead of a numerical solution of the Lyapunov equation[1]. Lall et al. proposed to use this way of Gramian estimation to reduce the dimension of complex, controlled non-linear systems by balanced truncation [19]. For linear systems, the integral for the computation of the controllability Gramian in Eq. 4 can be approximated by the sum of the outer product of m state snapshots at equally spaced time steps $(1t_s, 2t_s, ..., mt_s)$:

$$\mathbf{W}_c \approx \sum_{i=1}^{m}\sum_{j=1}^{p} \mathbf{x}_{i,j}\mathbf{x}_{i,j}^T t_s \tag{8}$$

Herein, $\mathbf{x}_{i,j}$ is the i-th snapshot of the state response to a unit Dirac impulse at input j. The observability Gramian is similarily approximated by the help of the adjoint system defined in Eq. 7:

$$\mathbf{W}_o \approx \sum_{i=1}^{m}\sum_{j=1}^{q} \bar{\mathbf{x}}_{i,j}\bar{\mathbf{x}}_{i,j}^T t_s \tag{9}$$

Here, $\bar{\mathbf{x}}_{i,j}$ denotes the i-th snapshot of the state response to a unit Dirac impulse at input $\bar{\mathbf{u}}_j$ of the adjoint system. With the obtained approximated Gramians, first an aproximately balanced transformation is made, followed by an truncation of the least controllable and observable states. The main drawback of using empirical Gramians is that many simulation snapshots are needed for a sufficiently high accuracy of the approximation. For aerodynamic systems which usually have many inputs and outputs, the number of simulations required is particularly high.

Proper Orthogonal Decompostion Especially in the area of fluid dynamic simulation, the POD has proven itself in the past as an effective method for model reduction. The original concept of the POD was presented by Pearson as a method for finding the "best-fitting“ straight line or plane for 2D or 3D point clouds [20]. With respect to large systems, one of the most important advancements is the POD by the method of snapshots presented by Sirovich [21]. The principal idea behind the POD is to perform a Galerkin projection of the vector space onto a subspace spanned by orthonormal basis vectors so that the approximation of a given set of simulation snapshots is optimal in a least square sense [16]. Therefore, a set of m state snapshots at different time steps resulting from simulations with the full order model is collected in the snapshot matrix $\mathbf{X}$:

$$\mathbf{X} = \frac{1}{m}\left[\mathbf{x}(t_1),\ \dots\ , \mathbf{x}(t_m)\right] \tag{10}$$

It can be shown that, in the finite-dimensional space, the solution for the optimal approximation are the eigenvectors of the correlation matrix $\mathbf{X}\mathbf{X}^T$ [22]. The largest eigenvalues correspond to the most suitable POD mode shapes regarding approximating the given dataset $\mathbf{X}$. Hence, a reduced order model is formed by using only the eigenvectors belonging to the k largest eigenvalues.

The method of snapshots proposed by Sirovich makes use of the positive semidefiniteness of the correlation matrix $\mathbf{X}\mathbf{X}^T$ [21]. When the number of snapshots m is smaller than the number of states n, the size of the eigenvalue problem can be reduced from $n \times n$ to $m \times m$ by computing the eigenvalues of $\mathbf{X}^T\mathbf{X}$.

The resulting m POD modeshapes $\mathbf{\Phi}_{\text{POD}} = [\phi_1, ..., \phi_m]$ are then found by:

$$\phi_j = \frac{1}{\sqrt{\lambda_j}}\mathbf{X}\mathbf{v}_j \quad , j = 1, ..., m \tag{11}$$

where λ and $\mathbf{v}$ are the eigenvalues and eigenvectors of $\mathbf{X}^T\mathbf{X}$.

As the resulting modes are optimal in approximating a given dataset, the question remains if the same modes are suitable for the representation of the system dynamics.

Balanced Proper Orthogonal Decompoistion As the POD is based on snapshots of states, only the input-state behaviour is reflected in the resulting model. When empirical Gramians are used for a BT, additional snapshots of the impulse responses of the adjoint system have to be computed. This results in a large number of simulations required, especially when the number of outputs is large. To overcome these issues, Rowley suggested a combination of the BT and the POD which will be outlined in the following[4].

In the BPOD, first the m state snapshots $\mathbf{x}$ obtained from p impulse response calculations at time steps $t_1, ..., t_m$ are stored in the matrix $\mathbf{X} \in \mathbb{R}^{n \times pm}$ together with their appropriate quadrature coefficients $\delta_1, ..., \delta_m$, which are equal to the time interval between the individual snapshots (e.g. $\delta_i = t_i - t_{i-1}$):

$$\mathbf{X} = [\mathbf{x}_{1,1}\sqrt{\delta_1},\ \ldots\ , \mathbf{x}_{1,m}\sqrt{\delta_m},\ \ldots\ , \mathbf{x}_{p,m}\sqrt{\delta_m}] \tag{12}$$

When the number of outputs is large, it is recommended to first project the system output on POD modes generated from a dataset of input-output trajectories. As the input-state snapshots $\mathbf{X}$ are already computed, multiplication with the matrix $\mathbf{C}$ generates a set of input-output snapshots $\mathbf{Y}$:

$$\mathbf{Y} = \mathbf{C}\mathbf{X} \tag{13}$$

The eigenvectors and eigenvalues of $\mathbf{Y}^T\mathbf{Y}$ are used to define the POD output mode shapes $\mathbf{\Phi}_{\text{POD,o}}$ as it is shown in Eq. 11. The number of POD modes used for output projection h is given by the desired approximation error defined as:

$$\epsilon_{\text{proj}} = \sum_{j=h+1}^{q} \lambda_j \tag{14}$$

in which λ are the eigenvalues of $\mathbf{Y}^T\mathbf{Y}$.

Subsequently the input vector of the adjoint system $\bar{\mathbf{u}}$ in Eq. 7 is projected on the POD output modeshapes ($\bar{\mathbf{u}} = \mathbf{\Phi}_{\text{POD,o}}\check{\mathbf{u}}$):

$$\dot{\bar{\mathbf{x}}} = \mathbf{A}^T\bar{\mathbf{x}} + \mathbf{C}^T\mathbf{\Phi}_{\text{POD,o}}\check{\mathbf{u}} \tag{15}$$

Now, impulse response snapshots of the transformed adjoint system are taken at l time steps and stored in the matrix $\bar{\mathbf{X}} \in \mathbb{R}^{n \times hl}$

$$\bar{\mathbf{X}} = [\bar{\mathbf{x}}_{1,1}\sqrt{\delta_1},\ \ldots\ , \bar{\mathbf{x}}_{1,l}\sqrt{\delta_l},\ \ldots\ , \bar{\mathbf{x}}_{h,l}\sqrt{\delta_l}] \tag{16}$$

The transformation that approximately balances the system is then found by an SVD of $\bar{\mathbf{X}}^T\mathbf{X}$:

$$\bar{\mathbf{X}}^T\mathbf{X} = \mathbf{U}_b\mathbf{\Sigma}_b\mathbf{V}_b^T \tag{17}$$

$$\mathbf{\Phi}_{\text{bal}} \approx \mathbf{\Phi}_{\text{bal,a}} = \mathbf{X}\mathbf{V}_b\mathbf{\Sigma}_b^{-0.5} \tag{18}$$

$$\mathbf{\Phi}_{\text{bal}}^{-1} \approx \mathbf{\Phi}_{\text{bal,a}}^{-1} = \mathbf{\Sigma}_b^{-0.5}\mathbf{U}_b^T\bar{\mathbf{X}}^T \tag{19}$$

The ROM is then found by using only the first k columns of $\mathbf{\Phi}_{\mathrm{bal,a}}$ and the first k rows of $\mathbf{\Phi}_{\mathrm{bal,a}}$. Compared to the simple use of empirical Gramians, the method is especially useful when the number of states and outputs is large. The computation of the POD mode shapes for output projection requires only little extra computational effort as no additional impulse response simulations are necessary. However, during the analyses run for this paper, it has been observed that the matrices $\mathbf{X}$ and $\bar{\mathbf{X}}$ can get very large and the product $\bar{\mathbf{X}}^T\mathbf{X}$ may get prohibitively expensive when it comes to memory usage. In this case and more specifically when $pm > n$ or $hl > n$, it is more efficient to compute a form of approximated Gramians by:

$$\mathbf{W}_c \approx \mathbf{X}\mathbf{X}^T \tag{20}$$

$$\mathbf{W}_o \approx \bar{\mathbf{X}}\bar{\mathbf{X}}^T \tag{21}$$

Similar to the empirical Gramians discussed earlier, the accuracy of the Gramians strongly depends on the number of snapshots used in the impulse response simulation. The accuracy of the approximated observability Gramian additionally depends on the chosen projection error ϵ_{proj} used for the determination of POD modeshapes h used in the output projection (Eq. 14). With the use of these approximated Gramians, the balanced transformation and the reduced order model can be computed as described in the BT.

Contrary to the POD, the BPOD takes into account the input-state as well as the state-output dynamics for the selection of states that are kept in the reduced order model. In addition, it has been found that the BPOD shows higher robustness with regard to preserving stability compared to the POD [23]. Compared to the use of empirical Gramians, the BPOD reduces the amount of required impulse response simulations of the adjoint system by reducing the number of outputs prior to the training data generation process.

2.2 Synthetic Mode Shapes for Snapshot Data Generation in Aeroservoelastic Applications

In aeroservoelastic applications, the aerodynamic model is responsible for calculating distributed forces among the surfaces given the boundary conditions imposed at the same surfaces by structural, flight dynamic and control surface degrees of freedom. When the aerodynamic and structural models are initially set up, the number of inputs to the aerodynamic model depends on the number of stations at which the force and displacement transfer between the aerodynamic and the structural model is facilitated. Using all possible stations as inputs for the aerodynamic model order reduction by the BPOD, a large number of simulations needs to be carried out to estimate the Gramians. Transforming the inputs to the aerodynamic model on generalised coordinates reduces the number of inputs. Typically, the eigenmodes of the in vacuo structural model are used for the generalised coordinate basis alongside with the control surface modes for the given control surface layout. As the targeted application of the proposed method is sizing type aeroservoelastic optimisation, generalised coordinates in terms of structural mode shapes and the control surface layout are unknown at the time of the generation of the reduced order model, i.e. before the optimisation.

In this work, synthetic mode shapes are used for the reduction of the number of inputs to the aerodynamic model. In the following, three different methods for the synthetic mode shape generation for full aircraft configurations are proposed. It is assumed that the surface on which the aerodynamic forces are computed and the boundary conditions are imposed, is given as a spatially discretised domain as is usual for finite difference, element or volume methods. For the sake of simplicity, the following description is limited to surface representations of the wings only, i.e. no fuselage aerodynamics are modelled.

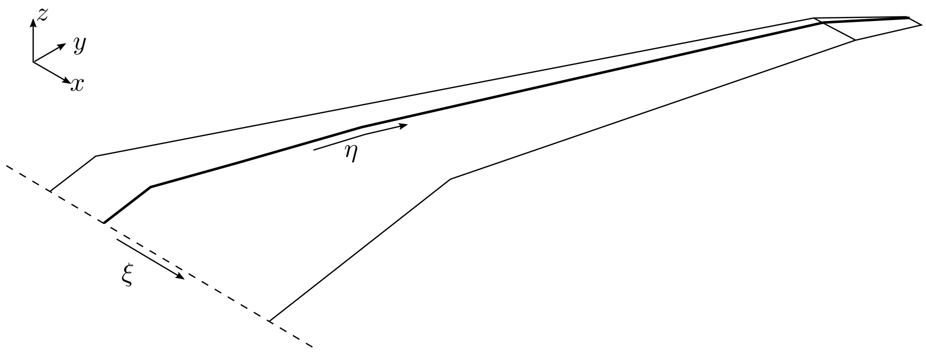

Figure 1: Location and definition of the introduced reference coordinate directions used for the formulation of the synthetic mode shapes on a lifting surface. The spanwise direction η follows the local one - quarter chord line and the chordwise direction ξ is placed along the primary flightpath.

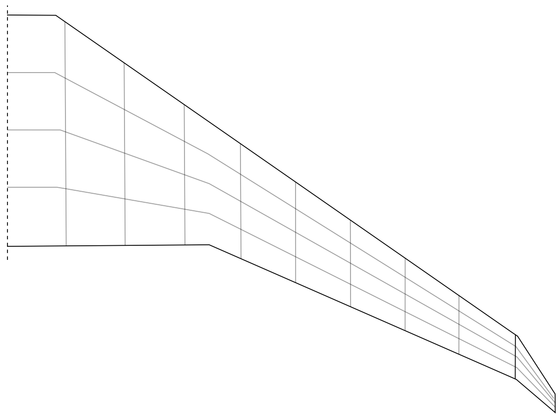

Figure 2: Example of the resulting zones for a division of the lifting surface $n_{z,\xi} = 4$ zones per chord and $n_{z,\eta} = 20$ zones per reference span.

Synthetic mode shapes based on Subdivision The first method used in this work is to divide each lifting surface into zones by spanwise as well as chordwise subdivision. To divide the lifting surfaces into zones, first, two reference coordinate directions per lifting surface are defined as shown in Fig. 1. A spanwise coordinate direction η is defined along the one-quarter chord line of each lifting surface ranging from one tip ($\eta = -1$) to the other ($\eta = 1$) for symmetric lifting surfaces and from the root ($\eta = -1$) to the tip ($\eta = 1$) for non-symmetric lifting surfaces. The chordwise coordinate direction ξ is defined along the primary flight direction and ranges from the local leading edge ($\xi = -1$) to the trailing edge ($\xi = 1$). The zones are then defined by dividers which are equally spaced along the two defined directions. As an example, Fig. 2 shows the resulting subdivisions for $n_{z,\eta} = 20$ zones per reference span as well as $n_{z,\xi} = 4$ zones per chord. For each zone, a synthetic mode shape is then defined by a vector with zeros for the boundary condition points which are outside and ones for the points which are inside the respective zone. Stacked horizontally, the mode shapes form the synthetic modal basis for the lifting surface. For the full aircraft configuration, the modal bases for each lifting surface are block-diagonally stacked. Depending on the number of subdivisions chosen, the transformation of the aerodynamic system results in a reduced number of inputs.

Gillebaart and De Breuker also used this approach to reduce the amount of impulse response simulations required to carry out the BPOD for a panel-based aerodynamic model. However, only one chordwise zone has been used while the spanwise number was chosen to be the number of spanwise panels used in the underlying aerodynamic full order model [7]. In this paper, the influence of the number of zones used on the resulting accuracy of the reduced order model is studied in Section 3..

Synthetic mode shapes based on Chebyshev Polynomials Another way of generating synthetic mode shapes is the use of spatial weighting functions. Ideally, the weighting functions form an orthogonal basis. One of the most

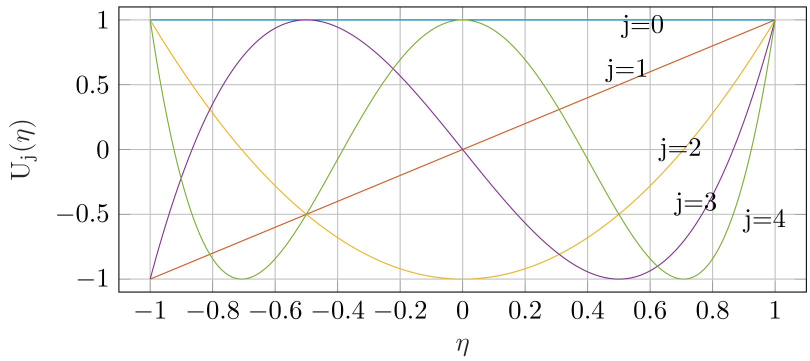

Figure 3: Chebyshev polynomials of the first kind as a function of η evaluated for various orders j.

prominent sets of orthogonal vectors are the Chebyshev polynomials of the first kind as shown in Fig. 3. An explicit definition of the one-dimensional polynomial in dependence of the order j is given as [24]:

$$U_j(\eta) = \frac{(\eta + \sqrt{\eta^2 - 1})^j + (\eta - \sqrt{\eta^2 - 1})^j}{2} \tag{22}$$

Again the two reference coordinate directions defined in Fig. 1 are used to formulate the mode shapes:

$$\begin{aligned} \phi_{c,(i-1)j+i}(\xi, \eta) =& U_i(\xi)U_j(\eta) \\ & \text{with } i = 0, ..., n_{c,\xi} - 1 \text{ and } j = 0, ..., n_{c,\eta} - 1 \end{aligned} \tag{23}$$

For a typical wing geometry, the resulting synthetic mode shapes for various orders are shown in Fig. 4. Again, the modes are horizontally stacked for each wing and block-diagonally arranged for the full aircraft configuration.

Winter et al. used a similar description for the generation of mode shapes [15]. However, in their formulation, the polynomials have been defined along global coordinate directions. As a result, the polynomial boundaries lie outside of the wings surface for tapered or swept wings. Hence, not the full weighting functions are used, and consequently, higher order polynomials are required to achieve the same distributions.

Synthetic mode shapes based on Radial Basis Functions The third set of synthetic mode shapes used in this work is based on radial basis functions. Here, the magnitude of the mode shapes depend on the distance to a centre node. The underlying formulation used in this work has been described by Zhang et al., however, adapted to be used for complex wing geometries [14]. First, the $n_{r,\xi}$ chordwise and $n_{r,\eta}$ spanwise centre nodes are placed equidistantly along each of the two reference coordinate directions defined in Fig. 1. The resulting centre nodes form a mesh in total consisting of $n_r = n_{r,\xi} n_{r,\eta}$ centre nodes. The i-th RBF is defined in dependence of the spanwise reference coordinate η as:

$$R_i(\eta) = (1 - d_\eta)^4(4d_\eta + 1) \tag{24}$$

Herein, d_η denotes the distance to the respective centre node in spanwise direction η defined as:

$$d_\eta = \max(\frac{|\eta - \eta_i|}{r_\eta}, 1) \tag{25}$$

with η_i being the spanwise station of the i-th centre node. The radius r is a function of a scaling factor f and the number of spanwise centre nodes:

$$r_\eta = \frac{f}{n_{r,\eta}} \tag{26}$$

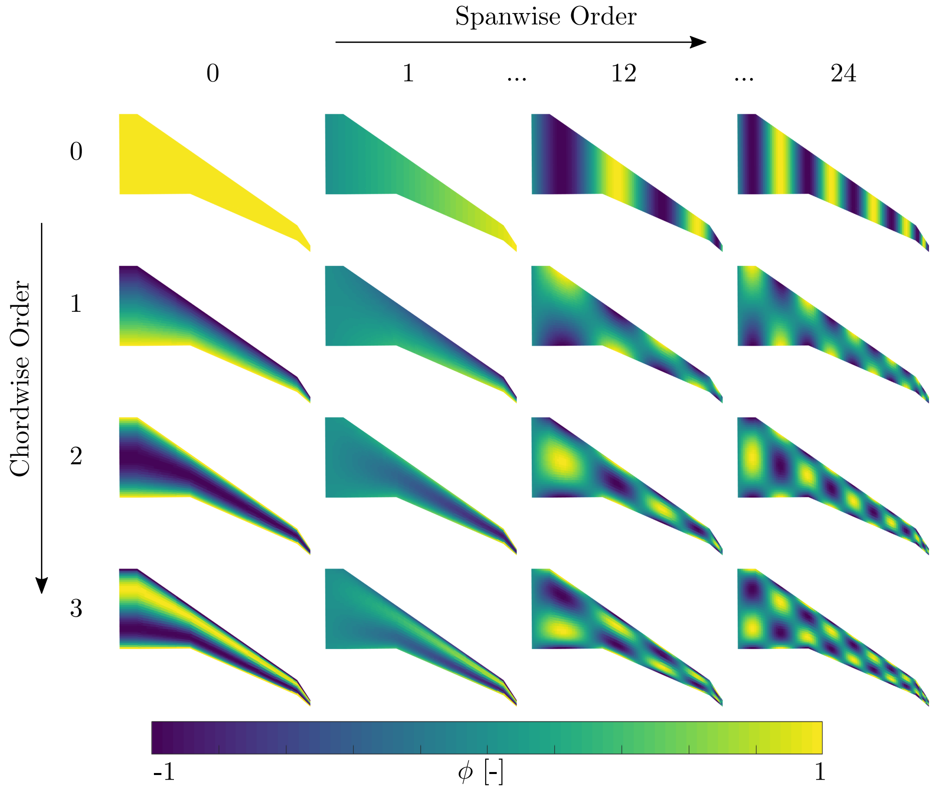

Figure 4: Synthetic mode shapes for a typical wing geometry based on Chebyshev polynomials of the first kind for various number of chordwise $n_{c,\xi}$ and spanwise polynomials $n_{c,\eta}$.

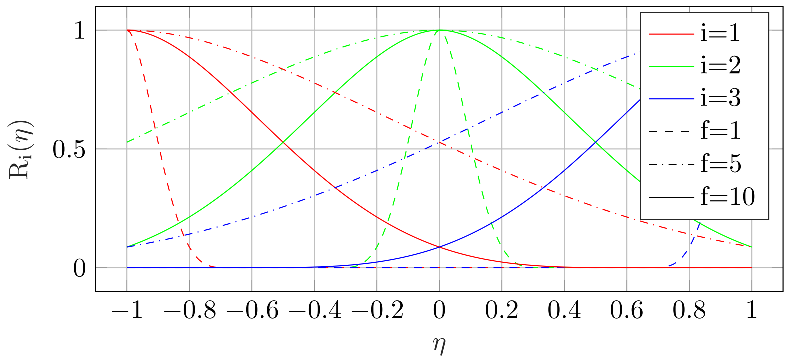

Figure 5: The resulting radial basis functions for a number of $n_r = 3$ centre nodes placed along the coordinate η for three different radius scaling factors f.

The resulting RBFs of $n_r = 3$ centre nodes are shown in Fig. 5 for different scaling factors f. Similarly, the RBF is defined in chordwise direction. One mode shape per centre node is then calculated by:

$$\begin{aligned}\phi_{r,i} =& R_i(\xi)R_i(\eta) \\ &\text{with } i = 1, ..., n_{r,\xi}n_{r,\eta}\end{aligned} \tag{27}$$

An example mode shape is shown in Fig. 6 alongside with the positions of the centre nodes for this case. Again, the mode shapes are stacked horizontally to form the transformation basis as for the other two methods described.

2.3 Resulting Process for Aerodynamic Model Order Reduction

The proposed process to create the reduced order aerodynamic model is summarised in the following steps:

1. Create a set of synthetic mode shapes $\mathbf{\Phi}_{\text{syn}}$ for the surfaces on which the aerodynamic model inputs are defined.
2. Project the input space of the aerodynamic model from Eq. 1 onto the chosen set of synthetic mode shapes to obtain the transformed ($\hat{}$) system with the input vector $\hat{\mathbf{u}}$:

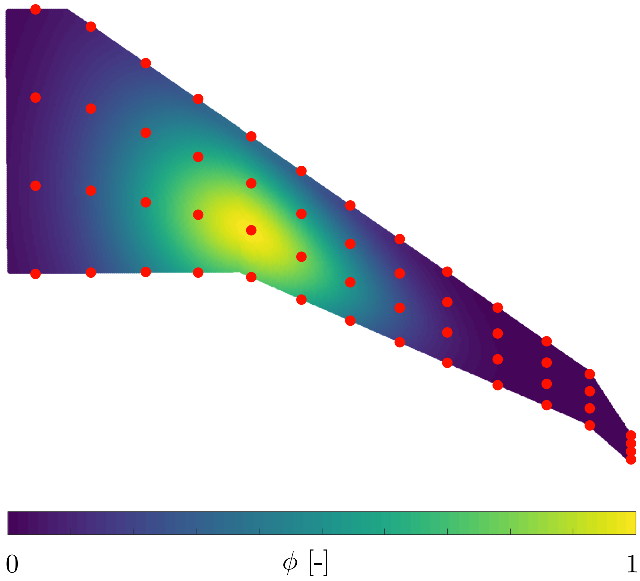

Figure 6: Example of a synthetic mode shape for a typical wing geometry based on radial basis functions alongside with the respective centre nodes.

$$\begin{aligned}\dot{\mathbf{x}} &= \mathbf{A}\mathbf{x} + \hat{\mathbf{B}}\hat{\mathbf{u}} = \mathbf{A}\mathbf{x} + \mathbf{B}\mathbf{\Phi}_{\text{syn}}\hat{\mathbf{u}} \\ \mathbf{y} &= \mathbf{C}\mathbf{x} + \hat{\mathbf{D}}\hat{\mathbf{u}} = \mathbf{C}\mathbf{x} + \mathbf{D}\mathbf{\Phi}_{\text{syn}}\hat{\mathbf{u}}\end{aligned} \tag{28}$$

3. Calculate the transformation $\mathbf{\Phi}_{\text{bal,a}}$ and $\mathbf{\Phi}^{-1}_{\text{bal,a}}$ that approximately balances the transformed system using the BPOD described in Sec. 2.1.

4. Select a subset of the balancing transformation to construct the reduction basis $\mathbf{\Phi}_r$ and $\mathbf{\Phi}_r^{-1}$ by keeping the firt k columns of $\mathbf{\Phi}_{\text{bal,a}}$ and the first k rows of $\mathbf{\Phi}^{-1}_{\text{bal,a}}$.

5. Transform the state space of the aerodynamic model with the reduction basis to obtain the k-th order ROM using Eq. 3.

Note, that no information concerning the structural or control surface properties is required for the generation of the aerodynamic ROM. In the following, the aerodynamic ROMs resulting from the proposed process are integrated with the structural and flight dynamic equations of motion and subsequently tested for their accuracy in aero(servo)elastic analyses. The synthetic mode shapes are only required for reducing the aerodynamic model and are not used in the integration of the aeroelastic model or the aero(servo)elastic analyses shown in the following.

3. Application and Results

In this section, first, the example case is introduced by describing the aeroservoelastic full order model with the structural and control surface variations used for benchmarking the resulting reduced order models (see Section 3.1). In Section 3.2, the aeroelastic analyses are introduced and appropriate error measures are defined to quantify the accuracy of the reduced order models in an objective comparison. The application of the BPOD without previous input transformation is described in Section 3.3. The main results produced with the proposed combination of the BPOD with input projection on synthetic mode shapes are presented in Section 3.4.

3.1 Model Description

As an illustrative example, a twin-engine tube wing aircraft configuration as depicted in Fig. 7a is examined. Since the resulting ROMs are to be used wit hin aeroservoelastic optimisation, they must be robust to structural and control

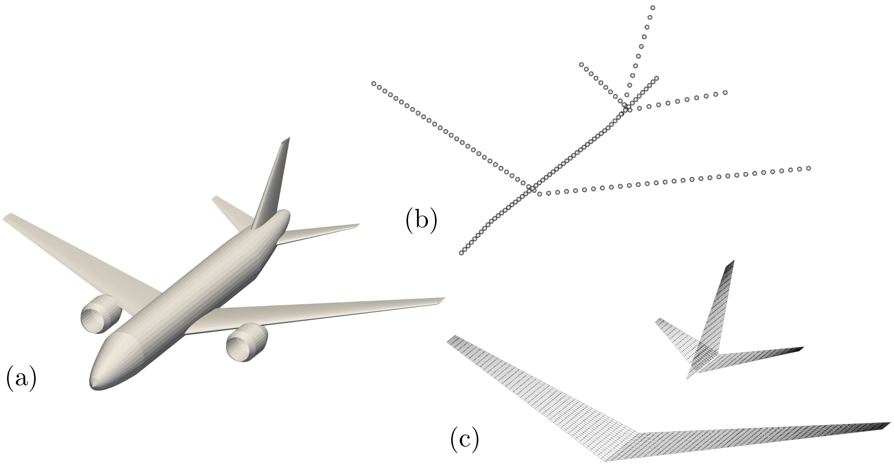

Figure 7: (a) The twin-engine tube wing aircraft configuration used as example. (b) The nodes representing the stick model used for the structural representation. (c) Panel mesh used for the generation of the full order unsteady aerodynamic model.

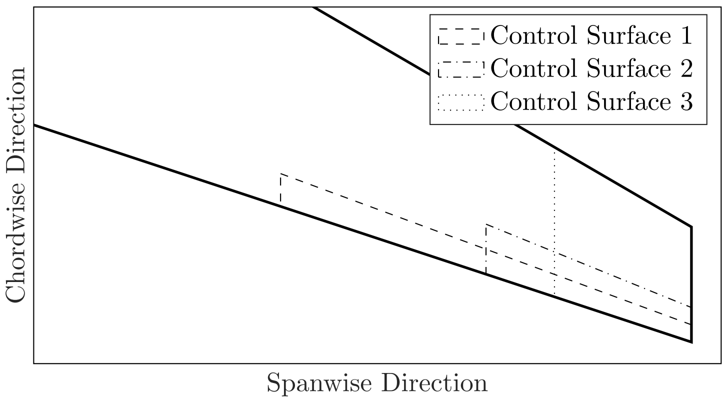

Figure 8: Schematic description of the three control surfaces used to test the robustness of the resulting ROMs regarding control surface layout variations.

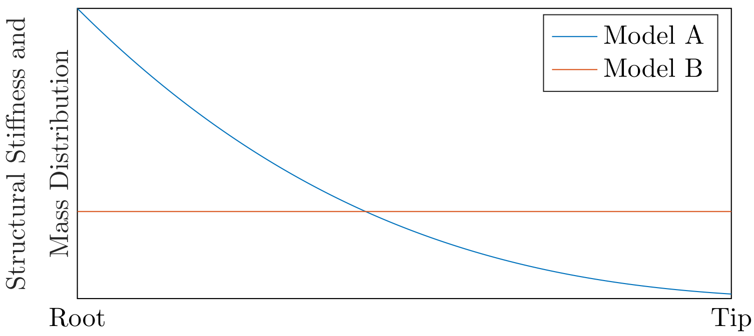

Figure 9: Primary stiffness and mass distributions of the two structural models used to test the robustness of the resulting ROMs regarding structural modifications.

Table 1: In vacuo structural mode frequencies of both structural models without the rigid body modes.

	Frequency [Hz]	
Mode	Model A	Model B
1	1.16	0.72
2	2.24	1.75
3	3.72	2.60
4	4.04	2.91
5	4.08	3.45
6	6.36	4.33
7	7.50	6.19
8	8.35	7.89
9	10.99	7.95
10	11.79	8.25

surface parameter variations. Therefore, three control surfaces are defined at the tip of the main wing, see Fig. 8), with chordwise lengths of 15, 30 and 100 % of the local chord and spanwise lengths of 30, 15 and 10 % of the span of the main wing.

The aerodynamic model is based on a continuous time state space formulation of the UVLM [25], [26]. The panel model consists of 2180 surface bound panels, see Fig. 7c, and 8580 wake panels. The resulting linear state-space model has 2180 inputs for the boundary conditions imposed at the panels, 8580 wake vorticity states and 2180 outputs for the pressures on the surface-bound panels. Deflection of the control surfaces is facilitated by rotation of the normal vectors in the area of the control surface. By appropriate weighting, the boundaries of the control surface do not need to coincide with the panels and can be moved without regenerating the panel mesh.

A practical mean axis formulation is used for the formulation of the equations of motion that introduce the flight dynamic rigid body degrees of freedom [27]. The structural model is based on Euler Bernoulli beam elements placed at the elastic axis of the wings and the fuselage. The nodes representing the structural beam model are shown in Fig. 7b. Two different structural models are defined for the aircraft configuration to evaluate the accuracy of the resulting ROMs in the presence of structural modifications. As shown in Fig. 9, Model A has cubic mass and stiffness distributions and for Model B, linear distributions are used for the wing and tail structure. Mass and stiffness along the fuselage are assumed to be constant for both models. These distributions were solely chosen to obtain different eigenmodes and are not comparable to any realistic designs. Large system masses (engine and landing gear) are modelled as concentrated masses with rigid lever arms. A total of 20 structural mode shapes is retained in the aeroelastic analyses. The frequencies of the first ten in vacuo structural modes are shown in Table 1 for both structural models.

3.2 Analyses and Accuracy Measures

The targeted sizing-type optimisation problem consists of objective and constraint functions that depend on the results of analyses carried out using the integrated aeroservoelastic model. In addition to flutter point and gust loads assessment, aeroservoelastic analyses include the analysis of dynamics involved by control surface motion. In the following, these analyses are described in more detail, and error measures for each aeroelastic analysis are derived which will be used for the evaluation of the accuracy of the resulting ROMs.

Flutter Point With both structural models, the testcase shows a flutter instability at subsonic speeds. A flutter analysis is performed for a constant Mach number of $\mathrm{Ma} = 0.5$ at sea level. Frequency ω and damping ζ of the first four structural modes over the velocity V are shown in Fig. 10 for model A and in Fig. 11 for model B.

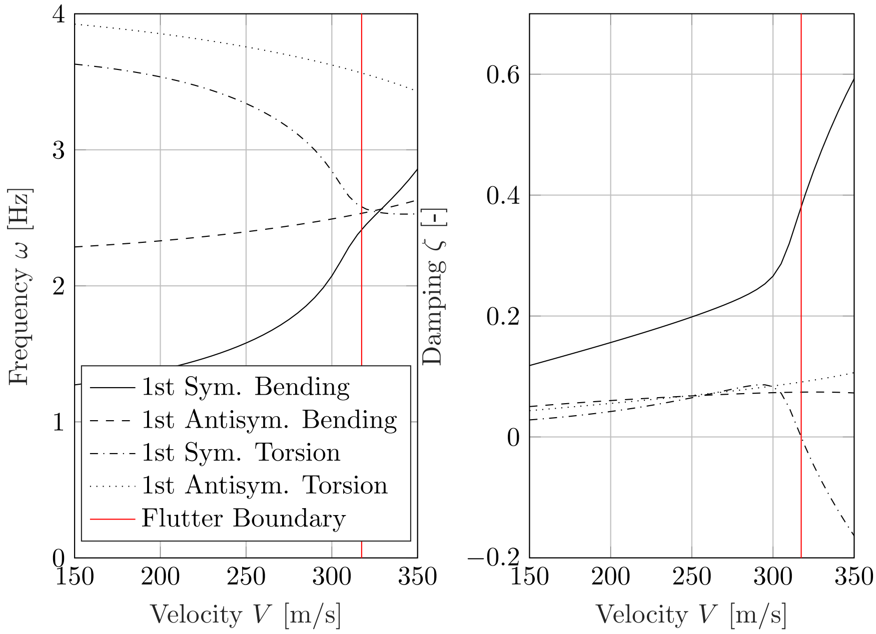

Figure 10: Flutter analysis results of the integrated aeroelastic model using structural Model A. The flutter boundary at a speed of $V = 317.37$ m/s is highlited.

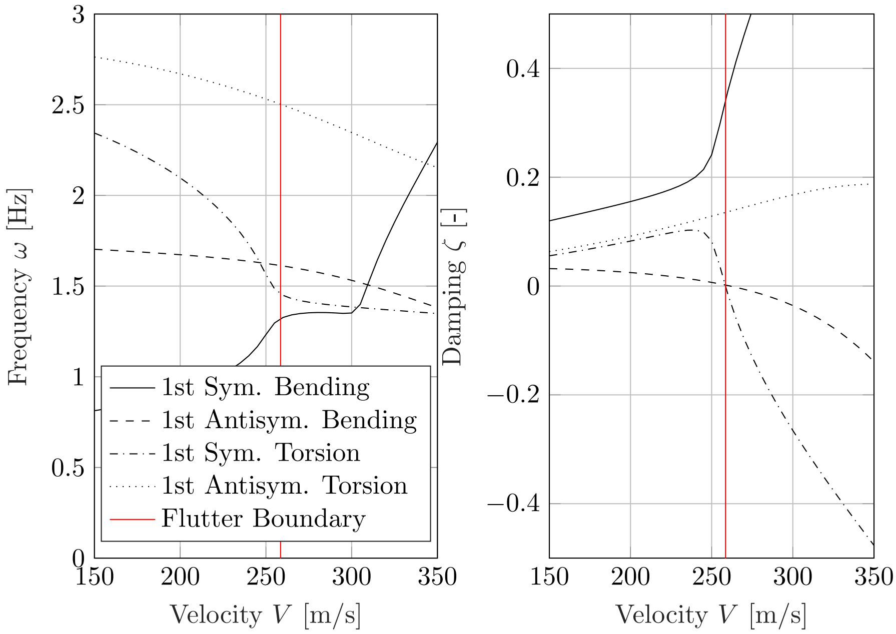

Figure 11: Flutter analysis results of the integrated aeroelastic model using structural Model B. The flutter boundary at a speed of $V = 258.55$ m/s is highlited.

The ROMs resulting from the proposed procedure shall be able to predict the flutter point (i.e. flutter speed and frequency) accurately for both structural models. In this work, the relative error in flutter speed V_f and frequency ω_f between every ROM ($\tilde{\cdot}$) and the unreduced, full order model is determined as:

$$\epsilon_{V_f} = \frac{\tilde{V}_f}{V_f} - 1 \tag{29}$$

$$\epsilon_{\omega_f} = \frac{\tilde{\omega}_f}{\omega_f} - 1 \tag{30}$$

The test case used shows a form of bending-torsion flutter with a high damping gradient near the flutter point. For flutter mechanisms in which the damping gradient is significantly lower, the flutter speed may vary strongly with small changes in the aeroelastic behaviour. For such flutter mechanisms, an error definition based on the damping of the aeroelastic modes of interest at a given speed should be used.

Gust Loads In this work, the root-mean-square (RMS) values of the dynamic response to a gust signal generated with the one dimensional von Kármán turbulence spectrum are used as a measure of the ROMs ability to predict gust loads. The parameters of the gust model are chosen according to the certification specifications for large aeroplanes [28]. A turbulence length scale of 2500 ft (762 m) is used, and the chosen flight condition corresponds to a Mach number of Ma = 0.5 at sea level which results in a turbulence intensity of 27.43 m/s. Gust zones are defined dividing the entire aircraft into 30 segments along the primary flight path to account for the time delay required as the vehicle passes through the gust. The error in the gust load prediction is defined as the relative difference in the RMS of the wing root bending moment $M_{x,\mathrm{wr}}$ between the ROM ($\tilde{\cdot}$) and the full order model:

$$\epsilon_{\mathrm{Gust}} = \frac{\mathrm{rms}(\tilde{M}_{x,\mathrm{wr}})}{\mathrm{rms}(M_{x,\mathrm{wr}})} - 1 \tag{31}$$

Control Surface Transfer Function As the intended application is an aeroservoelastic optimisation, the ROM used for the aerodynamics needs to accurately reproduce the influence of control surface motion on structural deflection and loads. Here, the influence is characterised by the transfer function from a symmetric control surface rotation input to an acceleration of the wing tip. The influence of actuation and sensor dynamics is not included in this transfer function. Error norms, such as the $\mathcal{H}_2$ norm, have been derived to measure the deviation of a given transfer function from a desired transfer function in the frequency domain. A frequency-limited formulation of the $\mathcal{H}_2$ norm is used which is given for a dynamical system G as [29]:

$$\|G\|_{\mathcal{H}_2,\omega,j} = \left(\frac{1}{\pi}\int_{\omega_1}^{\omega_2} |H_j(\nu)|^2 d\nu\right)^{\frac{1}{2}} \tag{32}$$

herein, H denotes the complex-valued transfer function from the control surface input j to the vertical tip acceleration. The frequencies ω_1 and ω_2 usually result from the targeted aeroelastic control law as well as the sensor and actuator bandwidth. The frequencies considered in this paper range from 1 to 250 rad/s. The transfer function (from the rotational input of control surface 2 to the wing tip vertical acceleration) of the aeroelastic model with the full aerodynamic model is shown in Fig. 12 in the frequency range considered for the error computation. It is noted, that for accurate reduced order modelling for lower frequencies of interest, the singular perturbation technique should be favoured over a simple truncation as used in this work. For more information on the singular perturbation technique, the reader is referred to [30].

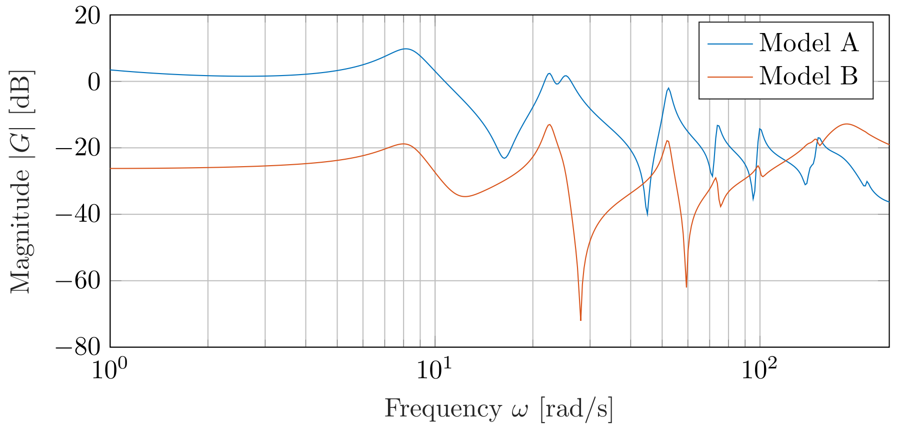

Figure 12: Transfer function from the rotational input of control surface 2 to the wing tip vertical acceleration. The transfer function is shown for both structural model variants and in the frequency range considered in the error computation.

To quantify the deviation between the transfer function resulting from the ROM $\tilde{G}$ and the full order model transfer function G, the control surface transfer function error ϵ_{CS} is calculated by:

$$\epsilon_{\text{CS}} = \frac{\|G - \tilde{G}\|_{\mathcal{H}_2,\omega}}{\|G\|_{\mathcal{H}_2,\omega}} \tag{33}$$

3.3 BPOD without Input Projection

Before applying the proposed combination of the BPOD with input projection on synthetic modes, a model reduction with the BPOD alone is presented in this section. Therefore all available inputs are used for the generation of the training data. With the presented test case, this results in 2850 input-state impulse response simulations required for the estimation of the controllability Gramian. The resulting state snapshots contain all possible characteristics that can be excited by the aerodynamic model inputs. To ensure that the subsequently calculated base of the POD modes contains all the relevant state characteristics, the projection error given in Eq. 14 is limited to $\epsilon_{\text{proj}} < 10^{-9}$. The approximately balancing transformation is computed with the approximation of the observability Gramian. In the following, aerodynamic ROMs are realised for various truncated model orders k and afterwards integrated with the structural and flight dynamic equations. These models are then used to perform the aeroelastic analyses described in the previous section. The calculation of the flutter point and gust loads results in two errors per structural model variant. Together with the three errors in the control surface transfer functions of the three control surfaces, this results in ve errors for each structural model variant or in a total of ten errors for both structural models investigated. The maximum among these errors ϵ_{max} over the truncated model order k is shown in Fig. 13. As usual for the balanced truncation, the maximum error decreases rapidly with increasing model order k. However, the maximum error is not necessarily decreasing monotonically. Instead, oscillations are possible, and therefore a monotonic decreasing envelope is calculated to improve the readability of all following plots. At low truncated model orders (less than $k = 50$), the aerodynamic ROMs do not contain enough dominant flow characteristics leading to high maximum errors in the aeroelastic analyses. With increasing truncated model order, the error decreases to $\epsilon_{\text{max}} = 4 \cdot 10^{-4}$ corresponding to the maximum achievable accuracy.

It is noted that contrary to a balanced truncation using exact gramians, the BPOD cannot yield the exact results even if the full order balancing transformation is used. The error can be explained by its three sources. First, the data used in the BPOD is based on discrete snapshots of continuous time signals. Second, the impulse responses are calculated for a finite time horizon. And Third, the inputs of the adjoint system are projected on a set of POD modes before the

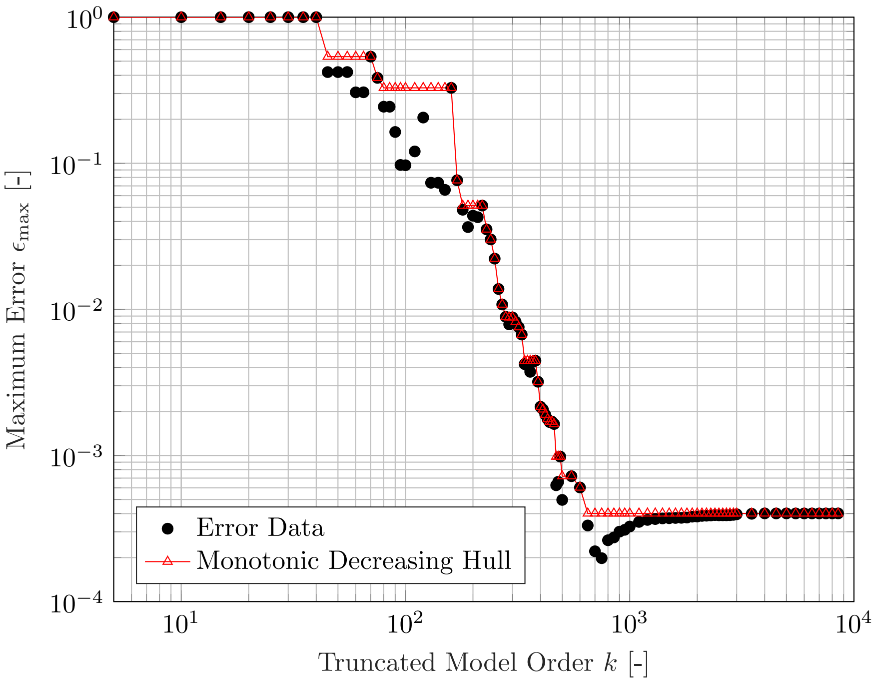

Figure 13: The maximum error (among the ten errors in the aeroelastic analyses) of the models resulting from a BPOD without input projection over the truncated model order. The monotonic decreasing envelope represents the upper expected error bound of the ROM.

Table 2: Maximum achievable accuracy and minimum model order required to achieve the desired accuracy of 0.1% in the different analyses and for the different structural models. The minimum achievable accuracy as well as the highest required minimum order are highlited. The models result from a BPOD without input projection.

Structural Model	Analysis		Achievable Accuracy	Required Order ($\epsilon < 10^{-3}$)
A	Flutter Speed		$1.46 \cdot 10^{-6}$	340
	Flutter Frequency		$7.86 \cdot 10^{-8}$	**470**
	Gust Loads		$1.46 \cdot 10^{-5}$	460
	Transfer Func.	Ctrl. Surf. 1	$2.33 \cdot 10^{-6}$	340
		Ctrl. Surf. 2	$2.39 \cdot 10^{-6}$	340
		Ctrl. Surf. 3	$2.18 \cdot 10^{-6}$	390
B	Flutter Speed		$1.14 \cdot 10^{-6}$	400
	Flutter Frequency		$1.88 \cdot 10^{-6}$	**470**
	Gust Loads		$\mathbf{4.01 \cdot 10^{-4}}$	370
	Transfer Func.	Ctrl. Surf. 1	$5.81 \cdot 10^{-6}$	**470**
		Ctrl. Surf. 2	$9.22 \cdot 10^{-6}$	**470**
		Ctrl. Surf. 3	$9.69 \cdot 10^{-6}$	**470**

determination of the observability Gramain. Consequently, if higher accuracy is desired, one may take more snapshots, increase the simulation time horizon and limit the output projection error ϵ_{proj} to lower values. The maximum achievable accuracy is sufficient for the studies in the present paper.

The error in the different analyses in dependency of the truncated model order k is shown in Fig. 14. Depending on the truncated model order, the highest error is caused by different analyses. While the highest error for low truncated model orders is observed in the flutter frequency, the maximum achievable accuracy is dominated by the gust load analysis. Without further studies, it is not evident whether the error is caused by the number of snapshots or by the end time of the impulse response simulations. The maximum achievable accuracies in all analyses with both structural models and all three control surfaces are listed in Table 2 together with the truncated model order required to achieve a given desired accuracy of $\epsilon < 10^{-3}$. For both structural models, the maximum achievable accuracy is driven by the gust load analysis. The required model order to achieve the desired accuracy is driven by the analysis of flutter frequency and control surface transfer functions both requiring a model order of $k = 470$.

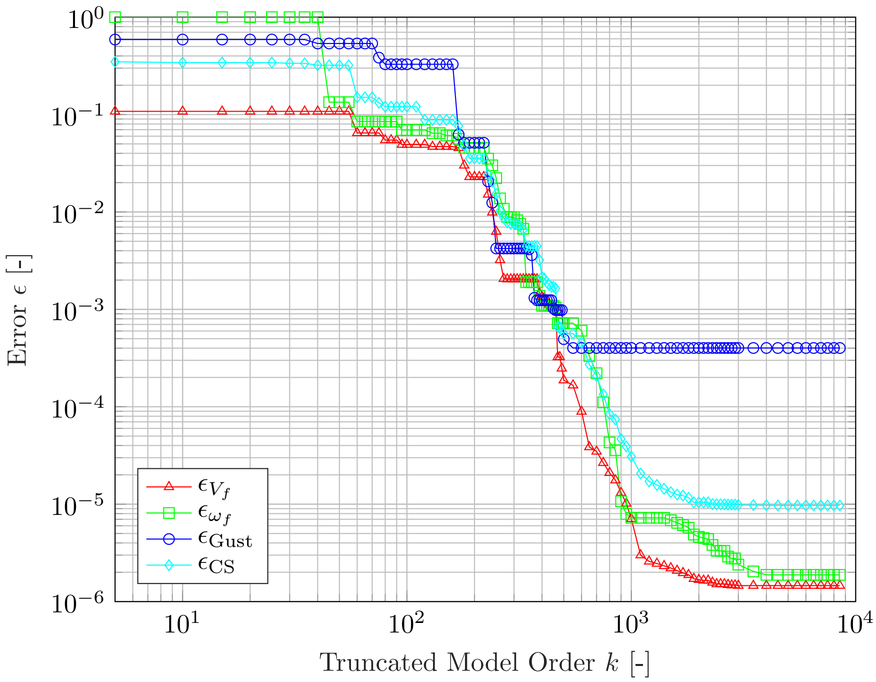

Figure 14: The analysis-specific error of the models resulting from a BPOD without input projection over the truncated model order.

3.4 BPOD with Input Projection on Synthetic Modes

The idea of the proposed method is to capture more relevant flow characteristics in less balancing modes by an input projection on a suitable set of synthetic modes before the BPOD. Thereby, the required model order to achieve the desired accuracy is minimised compared to the case without prior input projection.

For this, first, the optimal number of synthetic mode shapes is determined for each type of mode shapes separately in Section 3.4.1. In Section 3.4.2 the different types of mode shapes are then compared to each other concerning their suitability for the use in aerodynamic model order reduction. The results are also compared to the results without input transformation shown in the previous section.

3.4.1 The Optimal Number of Synthetic Modes

It is evident that with a larger number of orthogonal synthetic mode shapes, a closer approximation of the actual mode shapes can be obtained by linear combination. However, when more characteristics are included in the snapshot data used for the BPOD, the resulting singular values show a lower rate of decay, and thus less energy will be concentrated in or captured by the selected subset of balancing modes. As a result, for higher accuracy, larger subsets must be taken, and the resulting required model order is higher. Besides, a larger number of synthetic mode shapes results in more simulations that must be carried out leading to a higher computational effort required during the ROM generation phase. At the same time, a certain number of synthetic mode shapes is required to capture a sufficient variety of flow characteristics in the training data. The resulting reduced order model can only reflect characteristics which are available in the training data. In the following, ROMs are generated with varying numbers of synthetic mode shapes used in the process of snapshot data collection. The goal is then to find the right amount of synthetic modes needed to achieve a given desired accuracy in the aeroelastic analyses ($\epsilon_{\max} < 10^{-3}$) while keeping the computational effort for the model order generation and the required model order as low as possible.

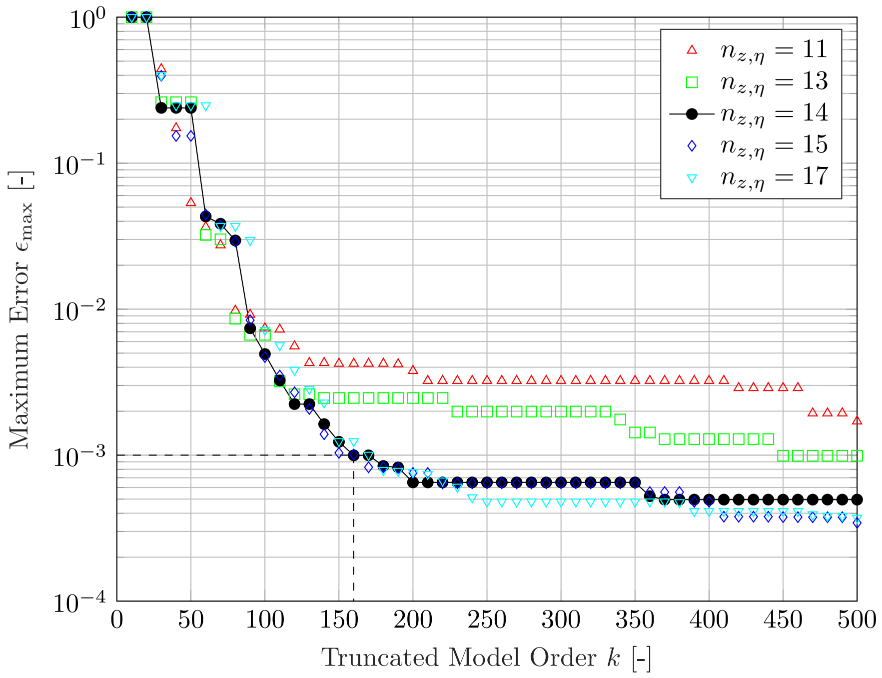

Figure 15: The maximum error in the aeroelastic analyses over the truncated model order for various number of zones per reference span $n_{z,\eta}$ at a fixed number of chordwise zones of $n_{z,\xi} = 2$.

Input Projection on Synthetic Modes based on Zonal Aggregation The maximum error over the truncated model order for the various number of zones per reference span $n_{z,\eta}$ at a fixed number of chordwise zones of $n_{z,\xi} = 2$ is shown in Fig. 15. As expected, the maximum error decreases rapidly with increasing truncated model order, i.e. the number of balancing modes kept in the transformation. The cases differ mainly in the maximum achievable accuracy within the analysed range of truncated model orders. More zones and thus more synthetic mode shapes result in a bigger and more complex set of data which contains a broader variety of state snapshots and therefore the rate at which the maximum error decreases, i.e. the accuracy per model order, is lower. It is furthermore observed, that if the number of synthetic mode shapes is too small, the captured characteristics are insufficient to achieve the desired accuracy.

For the given desired accuracy of $\epsilon_{\max} < 0.1\%$, both the cases $n_{z,\eta} = 14$ and $n_{z,\eta} = 15$ can be seen as optimal as both require the lowest truncated model to achieve the desired accuracy. However, a number of zones per reference span of $n_{z,\eta} = 14$ is chosen as a less computational effort is required for the generation of the ROM.

A similar behaviour can be observed when varying the chordwise number of zones $n_{z,\xi}$ at a fixed number of spanwise zones of $n_{z,\eta} = 14$. The resulting maximum error in the aeroelastic analyses over the truncated model order is shown in Fig. 16. Again, the case is identified which requires the lowest truncated model order to achieve the desired accuracy. With the additional constraint of keeping the number of synthetic modes as low as possible, a number of chordwise zones of $n_{z,\xi} = 2$ is identified as the most favourable case.

Input Projection on Synthetic Modes based on Chebyshev Polynomials The optimal number of Chebyshev modes is determined in the same way. The maximum error over the truncated model order for the various number of spanwise and chordwise Chebyshev polynomials is shown in Fig. 17 and Fig. 18. A similar trend is observed as in finding the optimal number of zones, and the optimal setup is chosen to be $n_{c,\eta} = 10$ and $n_{c,\xi} = 4$.

Input Projection on Synthetic Modes based on Radial Basis Functions Besides the number of RBF centre nodes, the formulation used for the generation

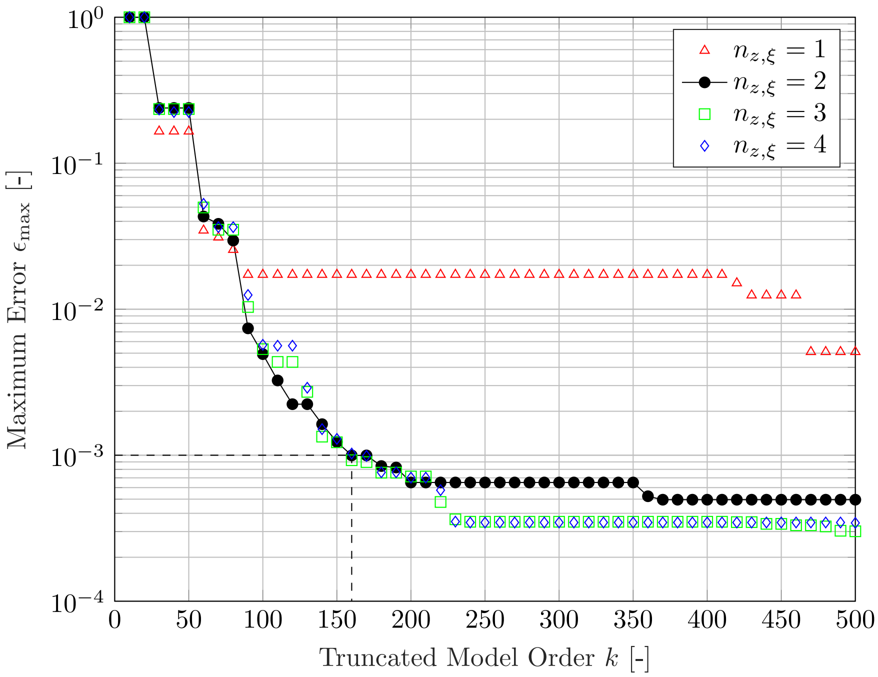

Figure 16: The maximum error in the aeroelastic analyses over the truncated model order for various number of chordwise zones $n_{z,\xi}$ at a fixed number of zones per reference span of $n_{z,\eta} = 14$.

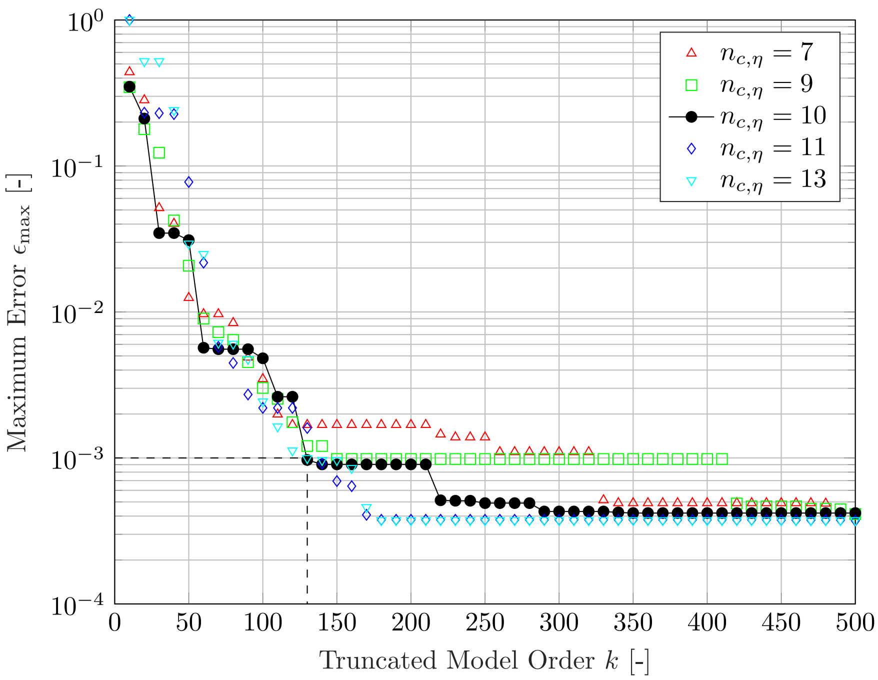

Figure 17: The maximum error in the aeroelastic analyses over the truncated model order for various number of Chebyshev polynomials per reference span $n_{c,\eta}$ at a fixed number of chordwise Chebyshev polynomials of $n_{c,\xi} = 4$.

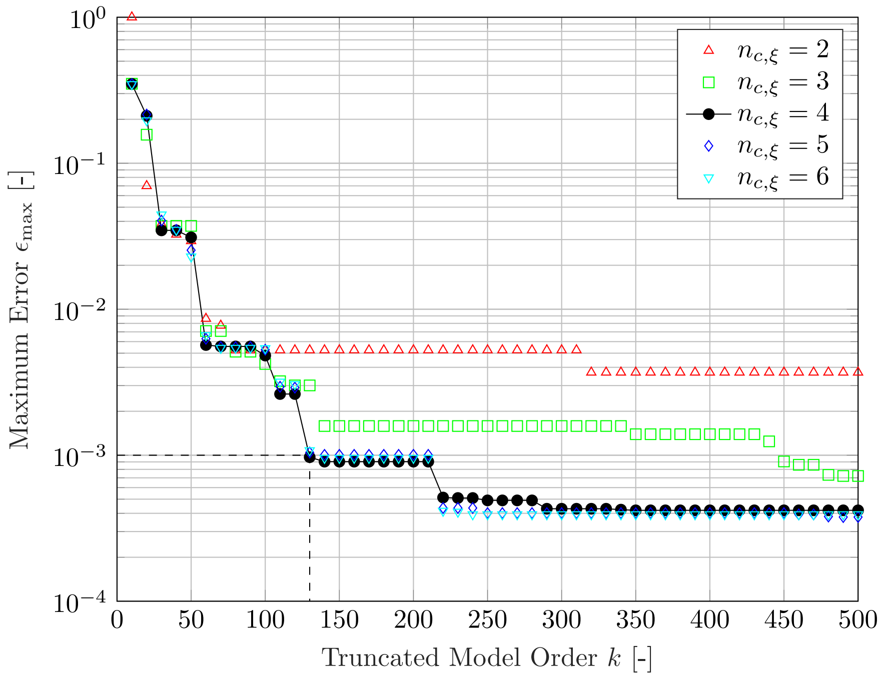

Figure 18: The maximum error in the aeroelastic analyses over the truncated model order for various number of chordwise Chebyshev polynomials of $n_{c,\xi}$ at a fixed number of Chebyshev polynomials per reference span of $n_{c,\eta} = 10$.

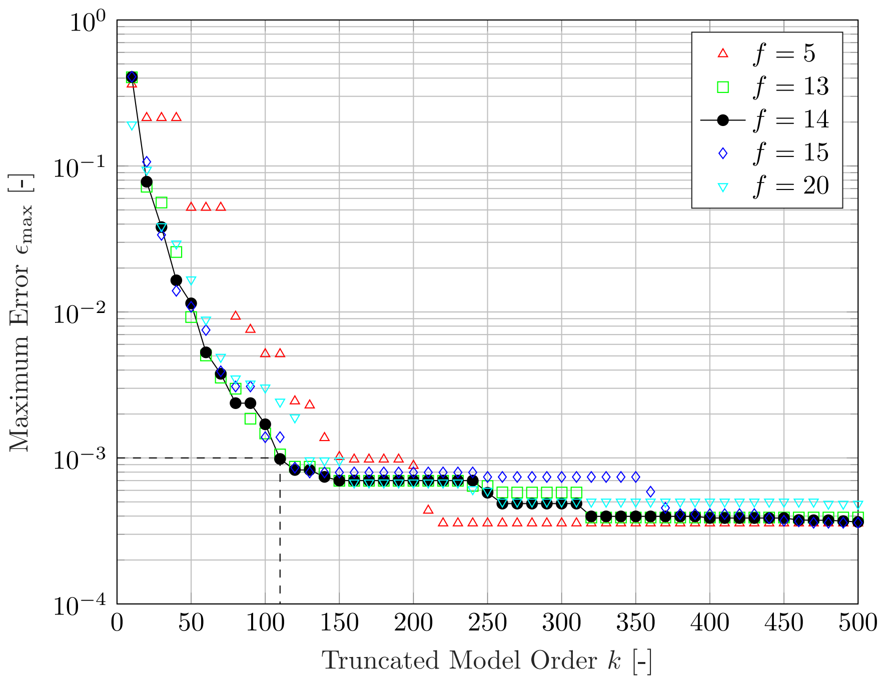

Figure 19: The maximum error in the aeroelastic analyses over the truncated model order for various radius scaling factors f at a fixed number of centre nodes per reference span of $n_{r,\eta} = 10$, and at a fixed number of chordwise centre nodes of $n_{r,\xi} = 4$.

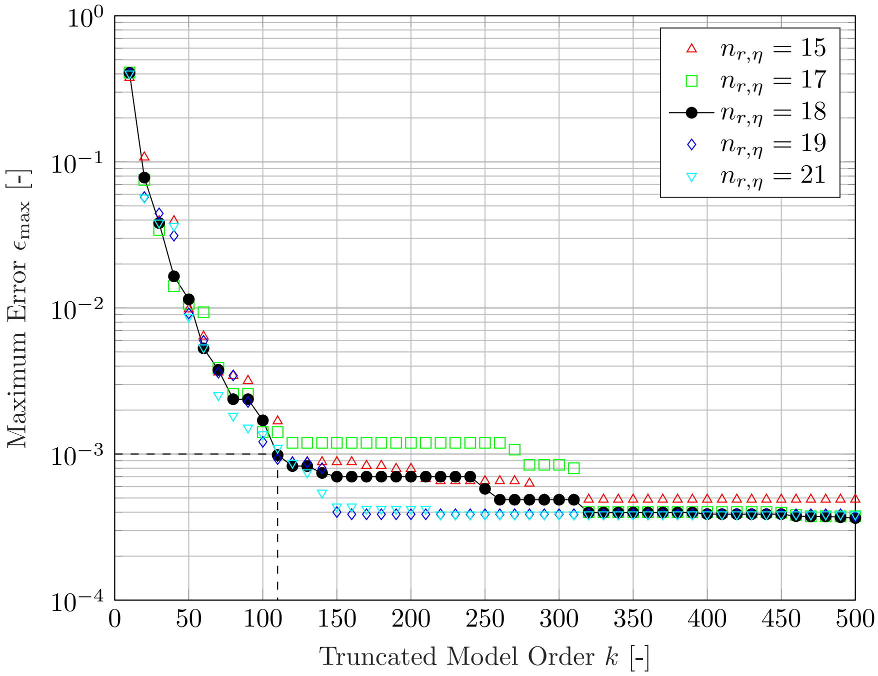

Figure 20: The maximum error in the aeroelastic analyses over the truncated model order for various number of centre nodes per reference span $n_{r,\eta}$ at a fixed number of chordwise centre nodes of $n_{r,\xi} = 3$ and a fixed radius scaling factor of $f = 14$.

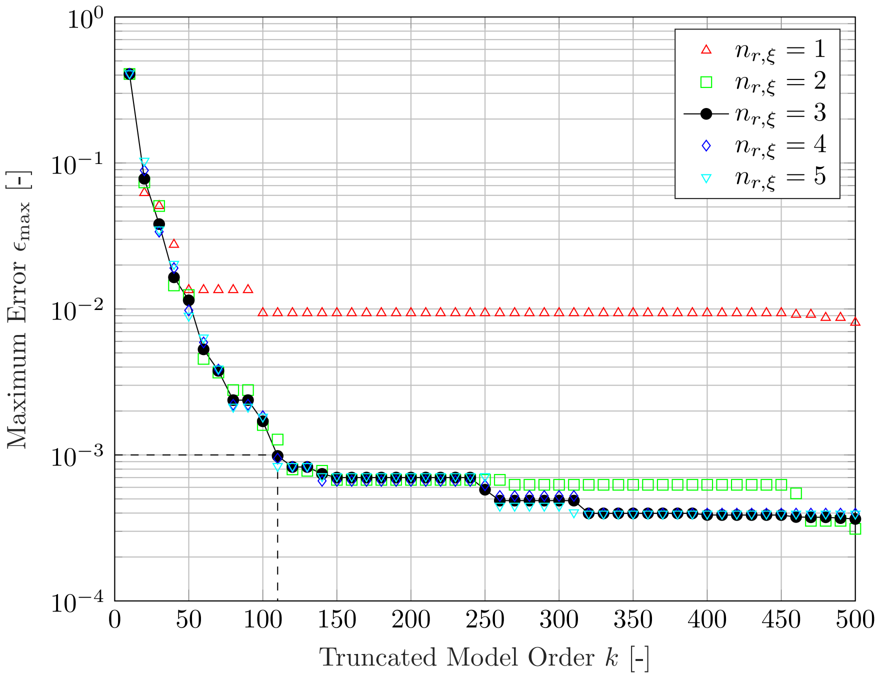

Figure 21: The maximum error in the aeroelastic analyses over the truncated model order for various number of chordwise centre nodes $n_{r,\xi}$ at a fixed number of centre nodes per reference span of $n_{r,\eta} = 18$ and a fixed radius scaling factor of $f = 14$.

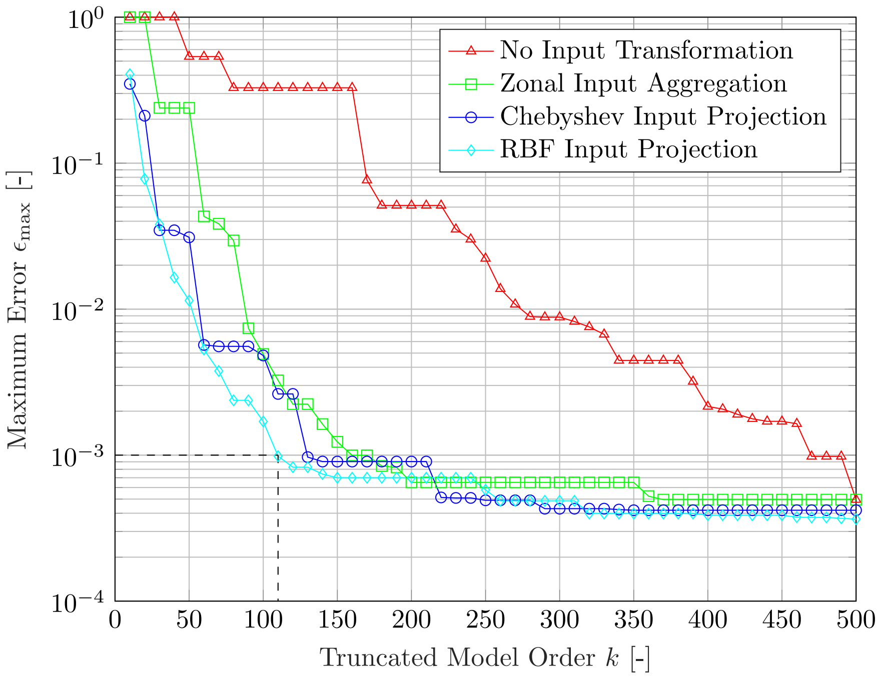

Figure 22: The resulting maximum error over the truncated model order for the different types of synthetic mode shapes used and a case without input transformation.

of RBF modes requires the definition of the radius scaling factor f in Eq. 26. The maximum error over the truncated model order for different radius scaling factors is shown in Fig. 19. Here, both the spanwise as well as the chordwise number of RBF centre nodes are fixed. Similar to the previously described way of determining the optimal number of synthetic mode shapes, the optimum radius scaling factor is found by identifying for which radius scaling factor f the lowest truncated model order is required. The maximum error over the truncated model order for the various number of spanwise and chordwise RBF centre nodes is shown in Fig. 20 and Fig. 21. The optimal setup is chosen to be $n_{r,\eta} = 18$ spanwise RBF centre nodes, $n_{r,\xi} = 3$ chordwise RBF centre nodes and a radius scaling factor of $f = 14$.

3.4.2 The Optimal Type of Synthetic Modeshapes

The individually chosen parameters for the synthetic mode shapes are optimal in terms of the compactness of the resulting ROMs for the given desired accuracy. In the following, the different sets are compared to each other to find the most suitable type of synthetic modes.

Accuracy per Order The resulting maximum error over the truncated model order is shown in Fig. 22 for the different types of synthetic mode shapes used. For comparison, results are also shown in which the balancing transformation is determined without prior input transformation as presented in Section 3.3. It can be immediately seen that with an input projection by each of the types of synthetic mode shapes, models can be established showing a higher accuracy per order in the analysed range of truncated model orders compared to the method without prior input transformation. Among the three methods employing synthetic mode shapes, the use of RBF modes shows the highest rate of decrease in the maximum error. Furthermore, the models created by using RBF modes show fewer oscillations in the error which can be seen by the fact that the monotonically decreasing envelope has fewer areas in which the error is constant over a range of truncated model orders. This shows that synthetic mode shapes based on RBFs are less sensitive to the choice of the truncated model order.

Structural Model	Analysis		No Input Projection	Zonal Modes	Chebyshev Modes	RBF Modes
A	Flutter Speed		340	90	50	60
	Flutter Frequency		**470**	140	100	70
	Gust Loads		460	**160**	80	70
		Ctrl. Surf. 1	340	120	90	80
	Transfer Func.	Ctrl. Surf. 2	340	140	**130**	100
		Ctrl. Surf. 3	390	150	100	**110**
B	Flutter Speed		400	120	80	60
	Flutter Frequency		**470**	**160**	70	100
	Gust Loads		370	120	80	70
		Ctrl. Surf. 1	**470**	140	**130**	100
	Transfer Func.	Ctrl. Surf. 2	**470**	150	**130**	**110**
		Ctrl. Surf. 3	**470**	150	110	**110**
	Maximum		**470**	**160 (-66%)**	**130 (-72%)**	**110 (-77%)**

Table 3: Comparison of the required truncated model order in the different aeroelastic analyses for the different types of synthetic mode shapes used for input transformation and the case without input transformation. The highest required model order for each type is highlighted indicating the minimum required order to obtain $\epsilon_{\max} < 10^{-3}$.

Table 4: Number of required impulse response simulations for the different types of synthetic mode shapes used for input transformation and the case without input transformation.

	No Input Transformation	Zonal Modes	Chebyshev Modes	RBF Modes
$n_{\text{sim, primal}}$	2180	52	72	96
$n_{\text{sim, dual}}$	391	64	66	53
$n_{\text{sim, total}}$	2571	**116 (-95%)**	138 (-95%)	149 (-94%)

The model orders required to achieve the desired accuracy in the different aeroelastic analyses are summarised in Table 3. The order required to achieve the desired accuracy in all analyses ranges from 110 to 160 for the different types of synthetic mode shapes used. Compared to the case without input transformation, this corresponds to a reduction in the required model order of 66-77%. Depending on the type of synthetic modes, the required order is driven by different analyses. Using zonal modes, gust loads and flutter analysis (depending on the structural model) drive the required model order. When using modes based on Chebyshev polynomials or RBF functions, the required order is determined by the analysis of the control surface transfer functions.

Putting the results in relation to the unreduced, full order model, the BPOD results in a significant total reduction of the states ranging from 98.1% combined with zonal modes to 98.7% combined with RBF modes while the maximum error in the aeroelastic analyses being less than 0.1% in the presence of significant structural and control surface parameter variations.

Computational Effort Not only the accuracy per order of the ROM can be improved, but also the computational effort required for the generation of the balancing transformation can be reduced using synthetic mode shapes. In Table 4, the number of required impulse response simulations is listed for the different synthetic mode shapes used in their optimal setups. The reduction in required impulse response simulations is comparable for all the methods and lies in the range of 95% compared to the process without input transformation. Among the methods that use synthetic modes, the most significant reduction in computational effort can be achieved with zonal modes. Compared to RBF modes, about 22% fewer simulations are needed. Depending on the number of analyses carried out with the reduced order model and the complexity of the full order model, the choice of the type of synthetic mode shapes has to be done based on the available generation time and the desired accuracy of the reduced order model.

Correlation of the Results to the Modal Assurance Criterion The MAC is widely used to quantify the similarity of two mode shapes. The MAC value between two mode shapes ϕ_1 and ϕ_2 is given by [31]:

$$\text{MAC} = \frac{|\phi_1^T \phi_2|^2}{(\phi_1^T \phi_1)(\phi_2^T \phi_2)} \tag{34}$$

The more correlation, the higher the MAC value. A MAC value of 1 indicates full similarity, i.e. ϕ_1 and ϕ_2 are the same vector except for a possible scaling.

To use the MAC values as an approximation quantification, first, the approximated mode shapes are calculated with the respective set of synthetic modes by finding the linear combination. In Fig. 23 the resulting mean MAC Values are depicted for the different synthetic modal bases used in the prior analyses (i.e. in their optimal setup). While all types of synthetic mode shapes successfully approximate the rigid body modes, the RBF modes outperform the other methods in approximating the structural mode shapes of both structural models. This correlates to the result of the previous section where the models created

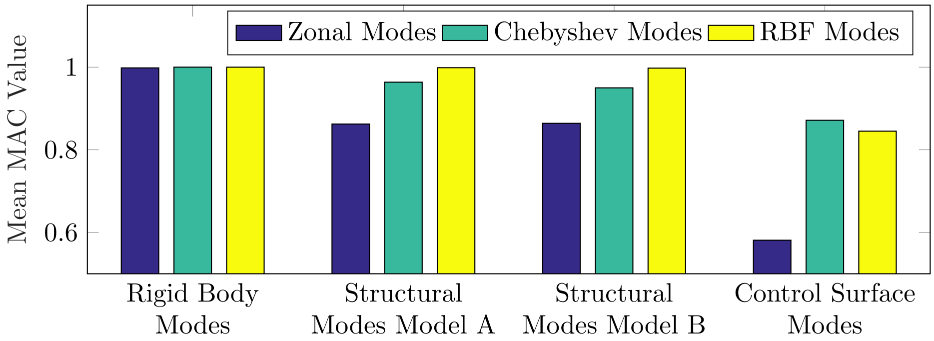

Figure 23: Mean MAC values between the actual mode shapes and the approximations resulting from the different sets of synthetic mode shapes in their optimal setup for model order reduction.

using RBF modes produce the highest accuracy per order. However, considering the MAC values of the control surface modes, no correlation is observed to the results shown in Table 3. Although the approximation of the control surface modes by RBF modes is not as accurate as by Chebyshev polynomials, the ROM produced using RBF modes still shows the highest accuracy per order in the control surface transfer functions. This becomes even clearer in the case of zonal modes. The MAC analysis shows a relatively poor consistency of the control surface modes compared to the structural and flight dynamic modes. In turn, the accuracy per order of the control surface transfer functions is comparable to the accuracy per order in the other aeroelastic analyses. In general, it can be said that evaluating the suitability of synthetic modes for the purpose of model reduction by the MAC value can be misleading and should be avoided.

4. Conclusion

In this work, a procedure for the generation of ROMs has been outlined which is suitable for the use in aeroservoelastic optimisation. The concepts of BPOD and synthetic mode shapes are combined to facilitate ROMs which are robust to structural and control surface layout variations. Three different types of synthetic mode shapes based on zonal subdivision, Chebyshev polynomials and RBFs have been formulated for full aircraft configurations. The resulting algorithm has been applied to an aeroservoelastic model of an exemplary aircraft configuration. Besides an analysis of the optimal number of synthetic mode shapes, the different types have been compared to each other concerning their accuracy in aeroservoelastic analyses, computational effort during the generation of the ROM and resulting MAC values.

It was shown that all methods are improving the accuracy per order of the resulting ROM compared to a BPOD without the use of synthetic mode shapes. Next, the influence of the number of synthetic modes used for the ROM generation was examined, with the result that the number of synthetic modes has a considerable impact on the achievable accuracy and the accuracy per order of the resulting ROM. The maximum error in the aeroelastic investigations (stability, gust loads and control surface transfer functions) caused by the model order reduction in the presence of structural and control surface layout variations has been constrained to be less than 0.1%. With this requirement, the optimal setup was determined for each type of mode shapes individually.

The use of RBF based mode shapes in combination with the BPOD resulted in the highest reduction of the states of 98.7% compared to the full order model and 77% compared to a BPOD without pror input transformation. To approximate the input space to the aerodynamic model, 96 RBF based synthetic mode shapes have been used. These mode shapes have been generated on a grid of ten points per reference span and four points per reference chord. The computational effort required for the generation of the ROM is reduced by 94% compared to the BPOD without input transformation. This generation time can be further reduced when using synthetic mode shapes based on zonal subdivision. The lowest required order for the desired accuracy was achieved with 14 zones per reference span and two zones per reference chord resulting in a total of 52 synthetic mode shapes used to approximate the input space of the aerodynamic model. The optimal type and number of synthetic mode shapes is thus depending on the envisaged number of simulations carried out with the reduced order model and the available time required for its generation.

The presented method was applied in the reduction of a linear, incompressible aerodynamic model based on the unsteady vortex lattice method. Analysing the capabilities of the method in reducing higher order aerodynamic models capturing complex flow effects (e.g. transonic effects) is subject to further research. However, since the excitation of the aerodynamic model is purely based on the structural and control surface motion, it is believed that the synthetic mode input projection still enhances the results and efficiency of model order reduction techniques based on simulation snapshot data.

References

[1] B. Moore, "Principal component analysis in linear systems: Controllability, observability, and model reduction," *IEEE Transactions on Automatic Control*, vol. 26, no. 1, 1981. https://doi.org/10.1109/TAC.1981.1102568.

[2] E. Livne, "Integrated aeroservoelastic optimization: Status and direction," *Journal of Aircraft*, vol. 36, no. 1, pp. 122–145, 1999. https://doi.org/10.2514/2.2419.

[3] G. Berkooz, P. Holmes, and J. L. Lumley, "The proper orthogonal decomposition in the analysis of turbulent flows," *Annual Review of Fluid Mechanics*, vol. 25, no. 1, 1993. https://doi.org/10.1146/annurev.fl.25.010193.002543.

[4] C. W. Rowley, "Model reduction for fluids using balanced proper orthogonal decomposition," *International Journal of Bifurcation and Chaos*, vol. 15, no. 03, pp. 997–1013, 2005. https://doi.org/10.1142/S0218127405012429.

[5] Z. Ma, S. Ahuja, and C. W. Rowley, "Reduced order models for control of fluids using the eigensystem realization algorithm," *Theoretical and Computational Fluid Dynamics*, vol. 25, no. 1-4, pp. 233–247, 2011. https://doi.org/10.1007/s00162-010-0184-8.

[6] T. B. Thanh and K. Willcox, "Model reduction for large-scale cfd applications using balanced proper orthogonal decomposition," *17th AIAA Computational Fluid Dynamics Conference*, 2005. https://doi.org/10.2514/6.2005-4617.

[7] D. Rajpal, E. Gillebaart, and R. De Breuker, "Preliminary aeroelastic design of composite wings subjected to critical gust loads," *Aerospace Science and Technology*, no. 85, pp. 96–112, 2019. https://doi.org/10.1016/j.ast.2018.11.051.

[8] C. L. Fenwick, D. P. Jones, and A. L. Gaitonde, "Consideration of reduced order model interpolation for aeroelastic design using structural modification," *18th AIAA Computational Fluid Dynamics Conference*, 2007. https://doi.org/10.2514/6.2007-3831.

[9] M. Karpel, "Multidisciplinary optimization of aeroservoelastic systems using reduced-size models," *Journal of Aircraft*, vol. 29, no. 5, pp. 939–946, 1992. https://doi.org/10.2514/3.46266.

[10] M. Karpel and D. Raveh, "Fictitious mass element in structural dynamics," *AIAA Journal*, vol. 34, no. 3, pp. 607–613, 1996. https://doi.org/10.2514/3.13111.

[11] M. Karpel, "Efficient vibration mode analysis of aircraft with multiple externalstore configurations," *Journal of Aircraft*, vol. 25, no. 8, pp. 747–751, 1988. https://doi.org/10.2514/3.45653.

[12] M. Karpel and B. Moulin, "Models for aeroservoelastic analysis with smart structures," *Journal of Aircraft*, vol. 41, no. 2, pp. 314–321, 2004. https://doi.org/10.2514/3.20514.

[13] R. Voss, L. Tichy, and R. Thormann, "A rom based flutter prediction process and its validation with a new reference model," *International Forum of Aeroelasticity and Structural Dynamics*, 2011.

[14] W. Zhang, K. Chen, and Z. Ye, "Unsteady aerodynamic reduced-order modeling of an aeroelastic wing using arbitrary mode shapes," *Journal of Fluids and Structures*, vol. 58, pp. 254–270, 2015. https://doi.org/10.1016/j.jfluidstructs.2015.07.007.

[15] M. Winter, F. M. Heckmeier, and C. Breitsamter, "Cfd-based aeroelastic reduced-order modeling robust to structural parameter variations," *Aerospace Science and Technology*, vol. 67, pp. 13–30, 2017. https://doi.org/10.1016/j.ast.2017.03.030.

[16] W. H. A. Schilders, H. Van Der Vorst, and J. Rommes, *Model Order Reduction: Theory, Research Aspects and Applications*. Springer, 2008. https://doi.org/10.1007/978-3-540-78841-6.

[17] M. G. Safonov and R. Y. Chiang, "A schur method for balanced-truncation model reduction," *IEEE Transactions on Automatic Control*, vol. 34, no. 7, pp. 729–733, 1989. https://doi.org/10.1109/9.29399.

[18] S. Gugercin and A. C. Antoulas, "A survey of model reduction by balanced truncation and some new results," *International Journal of Control*, vol. 77, no. 8, pp. 748–766, 2004. https://doi.org/10.1080/00207170410001713448.

[19] S. Lall, J. E. Marsden, and S. Glavaski, "Empirical model reduction of controlled nonlinear systems," *IFAC Proceedings Volumes*, vol. 32, no. 2, pp. 2598–2603, 1999. https://doi.org/10.1016/S1474-6670(17)56442-3.

[20] K. Pearson, "On lines and planes of closest fit to systems of points in space," *The London, Edinburgh, and Dublin Philosophical Magazine and Journal of Science*, vol. 2, no. 11, pp. 559–572, 1901. https://doi.org/10.1080/14786440109462720.

[21] L. Sirovich, "Turbulence and the dynamics of coherent structures. part 1: Coherent structures," *Quarterly of applied mathematics*, vol. 45, no. 3, pp. 561–571, 1987. https://doi.org/10.1090/qam/910462.

[22] P. Holmes, J. L. Lumley, G. Berkooz, and C. W. Rowley, *Turbulence, coherent structures, dynamical systems and symmetry*. Cambridge: Cambridge university press, 2012. https://doi.org/10.1017/CBO9780511919701.

[23] M. Ilak and C. W. Rowley, "Modeling of transitional channel flow using balanced proper orthogonal decomposition," *PHYSICS OF FLUIDS*, vol. 20, no. 3, 2008. https://doi.org/10.1063/1.2840197.

[24] F. T. Boesch and H. Prodinger, “Spanning tree formulas and chebyshev polynomials,” *Graphs and Combinatorics*, vol. 2, no. 1, pp. 191–200, 1986. https://doi.org/10.1007/BF01788093.

[25] N. P. M. Werter, R. De Breuker, and M. M. Abdalla, “Continuous-time state-space unsteady aerodynamic modeling for efficient loads analysis,” *AIAA Journal*, vol. 56, no. 3, pp. 905–916, 2018. https://doi.org/10.2514/1.J056068.

[26] S. Binder, A. Wildschek, and R. De Breuker, “Extension of the continuous time unsteady vortex lattice method for arbitrary motion, control surface deflection and induced drag calculation,” *International Forum on Aeroelasticity and Structural Dynamics*, 2017.

[27] M. R. Waszak and D. K. Schmidt, “Flight dynamics of aeroelastic vehicles,” *Journal of Aircraft*, vol. 25, no. 6, pp. 563–571, 1988. https://doi.org/10.2514/3.45623.

[28] N.N., “Cs25 - certification specifications and acceptable means of compliance for large aeroplanes.,” *https://www.easa.europa.eu/certification-specifications/cs-25-large-aeroplanes*, 2018. https://www.easa.europa.eu/certification-specifications/cs-25-large-aeroplanes.

[29] D. Petersson and J. Löfberg, “Model reduction using a frequency-limited h2-cost,” *Systems & Control Letters*, vol. 67, pp. 32–39, 2014. https://doi.org/10.1016/j.sysconle.2014.02.004.

[30] P. V. Kokotovic, R. E. O’Malley Jr., and P. Sannuti, “Singular perturbations and order reduction in control theory - an overview,” *Automatica*, vol. 12, no. 2, pp. 123–132, 1976. https://doi.org/10.1016/0005-1098(76)90076-5.

[31] R. J. Allemang, “The modal assurance criterion – twenty years of use and abuse,” *Sound and vibration*, vol. 37, no. 8, pp. 14–23, 2003.